A&A manuscript no.
(will be inserted by hand later)

Your thesaurus codes are:
07.03.02 D/Shoemaker-Levy 9

ASTRONOMY AND ASTROPHYSICS
28.2.1997

Secondary fragmentation of comet Shoemaker–Levy 9 and the ramifications for the progenitor's breakup in July 1992

Z. Sekanina, P. W. Chodas, and D. K. Yeomans
Jet Propulsion Laboratory, California Institute of Technology, 4800 Oak Grove Drive, Pasadena, CA 91109, U.S.A.

February 28, 1997

Abstract. Comprehensive analysis of discrete events of secondary fragmentation leads to a conceptually new understanding of the process of disintegration of comet Shoemaker-Levy 9. We submit that the jovian tidal forces inflicted extensive cracks throughout the interior of the original nucleus, but did not split it apart. The initial disruption was apparently accomplished by stresses exerted on the cracked object by its fast rotation during the early post-perijove period of time. We argue that this disruption was in fact a rapid sequence of episodes during July 1992 and gave birth to the 12 on-train, or primary, fragments: A, C, D, E, G, H, K, L, Q (later Q_1), R, S, and W. The discrete events of secondary fragmentation, which gave birth to the off-train fragments, are understood in this scenario as stochastic manifestations of the continuing process of progressive disintegration. Of the 13 considered off-train fragments, nine were secondary — B, F, G_2, M, N, P (later P_2 or P_{2a}), Q_2, U, and V — and four were tertiary (J, P_1, P_{2b}, and T). The separation parameters of 11 off-train fragments were determined. The vectorial distribution of separation velocities of these fragments shows a strong concentration toward a great circle, unquestionably an effect of the approximately conserved angular momentum of the progenitor comet since the time of its initial disruption. Also apparent is their clumping (except for P_1) to a segment along the great circle implying that the fragments were consistently released from one side of their parents, thus explaining for the first time why the off-train fragments preferentially appeared on one side of the nuclear train. In order to obtain a consistent solution, our model requires that the points of separation be on the antisolar side of the parent fragments, where thermal stresses are likely to enhance the effect of rotation, The episodes of secondary fragmentation are found to have occurred in a period of time from a few weeks to at least nine months after the close encounter with Jupiter in early July 1992 and the separation velocities ranged between 0.36 and 1.7 m/s. The spin-axis position is determined to have been nearly in the jovicentric orbit plane, which rules out the Asphaug-Benz-Solem strengthless aggregate model as a plausible breakup hypothesis. Since the separation velocities are rotational in nature, they cannot substantially exceed the critical limit for centrifugal breakup and offer an estimate for the original nuclear dimensions. The comet's nucleus is found to have been approximately 10 km in diameter and spinning rapidly, With the exception of PI and apparently also P_2 and F, no nongravitational deceleration was detected in the motions of the off-train fragments. Serious doubts are cast on continuing appreciable activity of any of these fragments. Indeed, when it was necessary to introduce a deceleration into the equations of motion, the effect appears to have been due to the action of solar radiation pressure on the centroid of centimeter-sized particulate in the disintegrating condensations.

Key words: comet Shoemaker-Levy 9 — secondary fragmentation — rotational vs. tidal breakup — parent comet's angular momentum

Send offprint requests to: Z. Sekanina

1. Introduction

When discovered in late March 1993, comet Shoemaker-Levy 9 had the appearance of a train of up to 21 almost perfectly aligned nuclear fragments. In our study of the comet's evolution during 1993, we reported that accurate positions of six of the fragments -- B, F, J, M, P, and T — were characterized by "distinct off-train deviations, to the north in projection onto the plane of the sky, with a clear tendency to increase with time" (Sekanina *et al.* 1994; hereafter referred to as Paper 1). The 1994 observations left no doubt that there were two separate groups of condensations — the *on-train* fragments and the *off-train* fragments. The on-train condensations included A, E, G (or G_1), H, K, L, Q (later Q_1), R, S, W, and apparently also C and D, whose status has remained somewhat unclear (Sekanina 1996). Besides J and M, which were not seen in 1994, the group of off-train condensations consisted

of B, F, G_2, N, PI, P_2 (later P_{2a} and P_{2b}), Q_2, T, U, and V, all of which were observed during at least limited periods of time in 1994, The motions of A, C, and D, along with those of the off-train fragments, are examined in this study, The objectives are to determine, to the extent possible, the sequence of discrete events that led to the formation of the off-train fragments and to establish, for each of them, the conditions at birth, the nature of its subsequent motion, the identity of its parent fragment, and the hierarchy of the progenitor comet's splitting. We also revisit the issue of temporal variations in the orientation of the nuclear train and address the ramifications that our results have for the processes leading to, and accompanying, the progenitor's splitting near Jupiter in July 1992. Examples of the fragmentation events that lagged by months the initial disruption (which we now suspect was itself a sequence of breakups) were published (Paper 1 and Sekanina 1996); preliminary results of our investigation were presented in a progress report (Sekanina *et al.* 1996).

2. Comet splitting and secondary fragmentation of comet Shoemaker–Levy 9

Splitting is a fairly common phenomenon among comets, but its detection is observationally difficult because companion nuclei are often diffuse objects with large short-term brightness variations. By the early 1980s, 21 comets were known to have split (Sekanina 1982), but in the past 15 years this number, including comet pairs, has grown to more than 30. Comet splitting is usually nontidal in nature, in which case the rate at which the nuclear components drift apart is determined primarily by the net difference between contributions from directed outgassing to the orbital momenta of the two objects. This difference is referred to as a differential nongravitational effect (Sekanina 1997 and the references therein). It is responsible for the characteristic configuration with all companions eventually lagging along the orbit behind the principal nucleus; the latter is the most persistent and apparently by far the most massive fragment. It is often the only one that ultimately survives the splitting, Orbital effects of the impulse acquired by a companion during a nontidal breakup and described by the separation velocity are fairly minor.

Comets whose splitting involves tidal forces behave differently (Sekanina 1997). We document below that comet Shoemaker-Levy 9 is a textbook case that illustrates the distinction between the fragment configurations for tidally and nontidally split comets. .4 conspicuous deviation from the expected fragment configuration for nontidally split comets is reflected in the brightness relations among the condensations of Shoemaker–Levy 9: the leading component A was one of the fainter components (e.g., Weaver *et al.* 1995), while the four brightest ones, G, K, L, and Q, were all near the middle of the nuclear train. The magnitudes of the impact phenomena were largely consistent with this evidence (Hammel *et al.* 1995).

Some basic characteristics of the dynamical histories of the fragments, including the conditions at the time of separation, can be recovered by modelling the relative motions of these objects. The major complication in the case of comet Shoemaker-Levy 9 is that many of the fragments were not born during July 1992, shortly after perijove, but subsequently, as products of a long sequence of discrete events, described in Paper 1 as *secondary fragmentation*. We use this term generically, even though some of the breakup episodes involving the off-train fragments did in fact give birth to tertiary products, as shown below,

3. Approach and analysis

The practical approach to fitting the observed motions of the nuclear components involved in the various events of secondary fragmentation consists in applying two critical software modules linked together: (i) a sophisticated ephemeris-determination code and (ii) an iterative least-squares differential-correction optimization procedure.

The ephemeris-determination program starts from the known orbital elements for the parent fragment (Chodas and Yeomans 1996, referred to hereafter as Paper 2). The program allows positional offsets of the daughter fragment from the parent fragment (either in right ascension and declination or as separation in position angle) to be calculated as functions of (i) the time of separation, (ii) the positional differences, at this time, from the parent fragment's center in three cardinal directions, (iii) the velocity of separation, again at this same time, from the parent fragment in three cardinal directions, and (iv) the deceleration, relative to the parent fragment, radially away from the Sun, which acts continuously between the times of separation and observation and varies as the inverse square of heliocentric distance. The three cardinal directions defined by the jovicentric orbit of the parent fragment are the radial (away from Jupiter), transverse, and normal directions of the right-handed RTN coordinate system. The mutual gravitational attraction of parent and daughter fragments is ignored.

The iterative differential-correction procedure, which makes use of software that solves the normal equations for an arbitrary number of unknowns, is employed to determine up to five parameters: these are the separation time, the three RTN components of the separation velocity, and the relative deceleration. The partial derivat ives of the offsets with respect to the individual parameters are calculated numerically as finite differences. Both the steps of variation, the convergence constraints, and the limit for the number of iterations can freely be selected and controlled by input. In practice, it is always necessary to prescribe a rejection cutoff for positional residuals in right ascension and declination; all the observations leaving residuals that exceed this limit are excluded from the solution. This procedure facilitates and speeds up the convergence. In order to determine the sensitivity of our

solutions to the dataset employed, up to three levels of the rejection cutoff were assumed in some cases — usually 0.4, 0.3, and 0.2 arcsec.

An important feature of the code for the differential-correction procedure is the option to solve for any combination of fewer than the five parameters, so that a total of $(2^5 - 1)$, or 31, different versions are available. This option proved most beneficial especially for testing purposes and in the early phases of the iterative procedure before the solution had "settled" around the optimum parametric values, or when the convergence had been slow or failing. In our computations we used this feature to considerable advantage when it became obvious that the introduction of a deceleration was almost always unnecessary. Thus, the results of this study are presented mostly in terms of *four-parameter* solutions, yielding the time of separation and the three components of the separation velocity . Further experimentation in cases in which the four-parameter solutions failed to converge showed that the next best approach was to change, stepwise, the time of separation from one run to the next while maintaining this parameter fixed in each run and solving only for the three separation-velocity components. This way, one could search for a "quasi-optimized" *three-parameter* solution that was calculated by interpolating the time of separation to yield the minimum value for the sum of squares of the positional residuals. We employed this approach on a number of occasions to determine the starting set of parameters for an optimized four-parameter solution, as well as to establish — in cases of convergence difficulties — whether or not the derived time of separation approximately coincided with the 1992 time of perijove. However, these quasi-optimized solutions were not incorporated in our table of results, which only includes the converging four-parameter (and occasionally five-parameter) solutions.

The computer output for each solution includes the starting values of the parameters, their corrections (which must all be zeros if the procedure has fully converged), the final parametric values, and, for each entry, the observed and the final calculated offsets, the residuals O -C, and the differences between the offsets calculated from the normal equations and from the orbit, which represent a standard test for the optimization procedure's convergence, The output also includes the sum of squares of the residuals, the mean residual, the predicted time of impact, and the right ascension and declination of the separation-velocity vector and of the directions to the Sun and Jupiter as seen from the primary fragment at the time of separation. The point of impact is defined as the impactor's crossing the 100-mbar level of Jupiter's atmosphere, following the model by Lindal *et al.* (1981).

One of the intriguing problems presented by this comet is the major structural differences among the fragments. This is suggested by the fact that while many of them survived until impact with no dramatic changes in their appearance, others disintegrated long before their collision with Jupiter. Fragments of the latter kind may have been much more common than suggested by evidence from ground-based observations and from visual inspection of images taken with the Hubble Space Telescope (HST). Application of a comprehensive digital search technique to the central regions of the HST images of several condensations in the nuclear train reveals the presence of isolated clumps of pixels of elevated signal, which were identified as additional visually unresolved fragments in the condensations (Sekanina 1995). The second most prominent object in condensation P_2 detected on digital maps from late January 1994 turned out to be nucleus P_{2b} that appeared distinctly on an HST image taken two months later (Weaver *et al.* 1995).

4. Individual events of secondary fragmentation

Since the employed technique begins with the orbital elements for the parent fragment, the question of its identity is the first task to be addressed. In practice, this is by no means an easy task and it is prudent that more than one potential parent be examined for most of the daughter fragments under consideration. The criteria used to discriminate among the various scenarios include the mean residual, the temporal distribution of residuals from the offsets, the degree of solution convergence, the number of observations involved and, especially, the constraints set by the breakup sequence and by the impact time when it is reasonably well established from the observations. With all else being equal, we prefer the solution that yields the lowest separation velocity. As remarked in Sect, 3, solutions that included a nongravitational deceleration almost never improved the quality of the representation of positional offsets of the fragments and usually led to meaningless results. The only exceptions are condensations P_1 (Sect. 4.11) and apparently also F (Sect. 4.5) and P_2 (Sect. 4.10).

The details on the converging four-parameter (and several five-parameter) solutions are presented in Table 1. The individual columns list: the daughter fragment; the parent fragment; the rejection cutoff and the degree of convergence; the time of separation; the total magnitude of the velocity of separation; its radial, transverse, and normal components (as defined in Sect. 3): the number of offset pairs employed and the RMS residual; the right ascension and declination of the separation-velocity vector and of the fragment-Sun vector at the time of separation; the angle γ between the fragment-Sun vector and the separation-velocity vector and the true anomaly of the parent fragment in its jovicentric orbit at that time. calculated as the angle subtended by the Jupiter-fragment vectors at perijove and at the time of separation: and, finally, the predicted impact time (as observed at the Earth) of the daughter fragment and the status oft he solution. The motions of some of the secondary and tertiary fragments relative to their parents are shown in Figs. 1-2.

Table 1. Selected four- and five-parameter solutions for secondary-fragmentation events of comet Shoemaker-Levy 9.

Fragment		Rejection cutoff (arcsec)/ Conver-gence	Time of separation, T_{sep} (TDB)	Velocity of separation (m/s)				Number of data/ RMS residual (arcsec)	Sepa-ration velocity: α_{sep}/ δ_{sep}	Sun's direc-tion: α_{Sun}/ δ_{Sun}	Angle γ^a/ Jovicen-anomaly, u^b	Predicted impact time, tric true 94 Jul (UTC)[c] (d: hr:min:s) / Status
				Total	Component							
Daugh-ter	Par-ent			V_{sep}	V_{rad}	V_{transv}	V_{norm}					
B	F"	0.3 adequate	92 Aug 15.3 ±11.0	0.92 ±0.11	–0.908 ±0.115	-0.014 ±0.012	-0.138 ±0.014	41 ±0.140	284?71 +11?95	352?62 -3?74	69?29 +172?40	17:02:58:52
	G[d]	0.4 adequate	92 Aug 30.1 ±9.7	1.58 ±0.11	-1.435 ±0.118	+0.364 ±0.082	+0.541 ±0.074	63 ±0.212	252.60 +9.29	353.41 –3.21	101.18 +173.43	17:03:02:19
	H	0.4 robust	92 Aug 12.4 *9.3	1.77 ±0.18	-1,684 ±0.186	+0.295 ±0.029	+0.464 ±0.034	43 ±0.208	255.69 +11.03	352.47 –3.84	97.38 +172.18	17:03:04:17
	H	0.3 robust	92 Aug 3.4 ±9.1	1.59 ±0. 19	-1,490 ±0.205	+0.266 ±0.036	+0.483 ±0.047	27 ±0.149	252.64 +10.85	352.01 –4.17	99.97 +171.18	17:03:03:34
	H	0.2 robust	92 Aug 3.1 ±5.9	1.57 ±0.13	–1.480 ±0.133	+0.240 ±0.020	+0.453 ±0.029	17 ±0.101	256.69 +10.37	352.00 -4.18	95.96 +171.15	17:03:01:36 ●
c	E	0.3 adequate	92 Aug 13.7 ±27.8	7).34 ±0.11	-0.334 ±0.109	+0.021 ±0.013	+0.020 ±0.008	50 ±0.128	264.00 +14.82	352.53 –3.80	89.55 +172.29	17:07:10:25
	E	0.2 adequate	92 Aug 14.6 *19.9	0.34 ±0.08	–0.340 ±0.077	+0.033 ±0.008	+0.030 ±0.007	37 ±0.093	262.09 +13.57	352.58 –3.76	91.36 +172.38	17:07:10:14
	G	0.3 adequate	92 Aug 5.2 ±10.8	0.93 ±0.14	–0.916 ±0.143	+0.095 ±0.019	+0.115 ±0.016	46 ±0.127	265.72 +10.92	352.10 -4.10	87.23 +171.42	17:07:06:29
	G	0.2 adequate	92 Aug 8.1 ±7.9	0.96 ● 0.10	–0.953 4cO.1O1	+0.103 ±0.011	+0.111 ±0.008	35 ±0.103	262.43 +12.15	352.25 –4.00	90.67 +171.75	17:07:08:26
	H	0.3 adequate	92 Jul 30.1 ±6.2	1.23 ±0.14	–1.227 ±0.139	+0.087 ±0.020	+0.037 ±0.015	40 ±0.145	268.57 +10.95	351.80 –4.33	84.20 +170.56	17:07:11:07 *
	H	0.2 adequate	92 Aug 6.2 ±5.6	1.38 ±0.11	–1.376 ±0.111	+0.119 ±0.014	+0.047 ±0.014	28 ±0.104	268.83 +10.98	352.15 –4.07	84.24 +171.53	17:07:10:28
D	E	0.3 weak	92 Aug 25.0 ±39.2	0.16 ±0.06	–0.157 ±0.058	+0.025 ±0.022	+0.044 ±0.017	31 ±0.137	256.34 +12.12	353.13 –3.40	97.35 +173.12	17:11:52:49
	H	0.3 adequate	92 Jul 23.6 ±11.6	0.96 ±0.25	-0.943 ±0.258	+0.135 ±0.021	+0.122 ±0.025	28 ±0.134	265.27 +6.42	351.50 –4.58	86.78 +169.23	17:11:47:47 *
	H	0.2 robust	92 Jul 29.7 ±8.5	1.09 ±0.16	–1.070 ±0.162	+0.142 ±0.014	+0.115 ±0.011	21 ±0.104	267.08 +7.73	351.78 –4.35	85.35 +170.48	17:11:47:26
F	G[d]	0.3 adequate	92 Nov 1.5 ±9.3	0.89 *0.05	-0.549 ±0.025	+0.407 ±0.076	+0.573 ±0.050	67 ±0.151	226.03 +5.26	357.07 –1.04	130.95 +175.64	18:00:38:58
	H[d]	0.3 robust	92 Ott 12.0 *6.6	1.47 ±0.04	-1.293 ±0.049	+0.448 ±0.020	+0.542 ±0.017	62 ±0.133	249.41 +8.91	355.86 –1.73	106.52 +175.11	18:00:37:28
	H[d]	0.2 robust	92 Ott 5.3 ±6.3	1.42 ±0.04	–1.242 ±0.046	+0.427 ±0.012	+0.547 ±0.008	44 ±0.101	245.58 +10.07	355.47 –1.96	109.92 +174.91	18:00:38:52
	K	0.3 robust	92 Aug 23.9 *5.4	1.76 ±0.07	-1.593 ±0.082	+0.400 ±0.016	+0.633 ±0.011	51 ±0.152	249.04 +10.38	353.08 –3.43	104.42 +173.05	18:00:49:20
	K[e]	0.3 robust	92 Aug 27.4 ±4.9	1.70 ±0.07	–1.668 ±0.072	+0.272 ±0.026	+0.216 ±0.059	66 ±0.157	266.73 +9.13	353.27 –3.31	87.12 +173.27	18:00:36:32 ●
	K′	0.2 robust	92 Aug 28.9 ±4.9	1.72 ±0.07	-1.690 ±0.073	+0.245 ±0.023	+0.191 ±0.051	38 ±0.109	267.95 +9.85	353.35 –3.25	86.03 +173.36	18:00:36:17
J	K	0.15 robust	92Sept 21.5 ±28.5	0.48 *0.12	–0.471 ±0.101	+0.035 ±0.144	+0.110 ±0.289	4 ±0.096	252.41 +20.89	354.67 –2.43	102.32 +174.45	19:02:22:55
	L	0.15 robust	92 Aug 16.5 ±23.4	0.87 ±0.24	–0.854 ±0.237	–0.076 ±0.133	–0.144 ±0.289	4 ±0.097	287'.35 +15.48	352.68 –3.70	67.41 +172.53	19:01:58:53
	N	0.15 robust	92 Aug 10.0 ±11.4	1.30 ±0.18	–1.252 ±0.185	+0.210 ±0.095	+0.298 ±0.211	4 ±0.069	260.14 +9.80	352.35 –3.93	92.84 +171.93	19:03:17:45 0
M	P[g]	0.15 adequate	92 Ott 18.7 ±23.4	0.70 ±0.17	- 0.645 ±0.113	+0.160 ±0.242	+0.206 ±0.430	4 ±0.133	248.74 +14.84	356.25 –1.50	107.30 +175.28	20:06:10:05
	Q	0.15 robust	92 Aug 31.0 ±24.5	1.00 ±0.24	–0.673 ±0.135	+0.312 ±0.153	+0.674 ±0.320	4 ±0.108	224.96 +10.20	353.46 –3.18	128.43 +175.28	20:07:16:51 ●
N	Q	0.3 adequate	92 Aug 17.7 ±0.3	0.63 ±0.01	–0.443 ±0.002	+0.196 ±0.013	+0.399 ±0.011	25[g] ±0.156	231.37 +7.38	352.75 –3.65	121.57 +172.61	20:10:29:19
	Q	0.2 robust	92 Aug 9.7 ±0.2	0.57 ±0.01	–0.402 ±0.001	+0.161 ±0.011	+0.378 ±0.009	139 ±0.089	230.24 +8.67	352.33 –3.94	122.30 +171.98	20:10:29:17 ●

Table 1 (continued).

Fragment: Daughter	Fragment: Parent	Rejection cutoff (arcsec)/ Convergence	Time of separation, T_{sep} (TDB)	Velocity of separation (m/s): Total v_{sep}	Component: V_{rad}	V_{transv}	V_{norm}	Number of data/ RMS residual (arcsec)	Separation velocity: α_{sep}/ δ_{sep}	Sun's direction: α_{Sun}/ δ_{Sun}	Angle -y"/ Jovicentric true anomaly, u^b	Predicted impact time, 94 Jul (UTC)[c] (d:hr:min:s)/ Status
P (P_2)	Q	0.3 adequate	92 Dec 25.7 ±7.1	1.23 ±0.08	–0.511 ±0.015	+0.674 ±0.090	+0.887 ±0.084	34 ±0.148	211.85 +6.27	0.39 +0.75	147.82 +176.68	20:15:19:47
	Q	0.2 adequate	92 Dec 14.5 ±6.4	1.14 ±0.03	-0.478 ±0.014	+0.585 ±0.050	+0.851 ±0.019	24 ±0.111	210.29 +8.62	359.70 +0.39	148,22 +176.50	20: 5:23:56
	Q'	0.2 adequate	92 Nov 4.9 ±10.5	0.50 ±0.05	-0.438 ±0.017	+0.126 ±0.080	+0.198 ±0.097	27 ±0.102	249.25 +13.47	357.28 –0.92	107.74 +175.72	20: 5:10:43 ●
	$Q^{i,j}$	0.05 robust	92 Dec 19.4 ±8.5	0.69 ±0.05	-0.555 ±0.019	+0.226 ±0.090	+0.3 ±0.082	3 ±0.038	241.27 +14.48	0.00 +0.55	117.58 +176.58	20: 4:45:16
P_1	P^k	0.3 weak	92 Nov 18.5 ±84.9	1.07 ±0.32	+0.030 ±0.050	-0.564 ±0.435	-0.904 ±0.262	16 ±0.135	9°94 –0°15	358°13 –0°46	11°81 +175°98	20:17:24:03
	$P^{i,l}$	0.05 robust	92 Nov 17.3 ±39.5	0.99 ±0.43	+0.039 ±0.023	-0.519 ±0.592	-0.840 ±0.361	3 ±0.046	10.37 –0.71	358.02 –0.51	12.35 +175.95	20:17:30:15 o
	$Q^{d,m}$	0.2 robust	93 Apr 8.1 ±21.4	0.98 ±0.20	-0.441 ±0.020	-0.825 ±0.112	–0.295 ±0.569	11 ±0.091	349.87 +32.95	7.06 +4.06	33.05 +178.04	20:16:40:43
	Q"i'"	0.1 robust	92 Dec 27.6 ±26.5	0.73 ±0.18	–0.509 ±0.042	–0.302 ±0.132	-0.422 ±0.299	3 ±0.090	326.04 +13.48	0.51 +0.82	36.39 +176.72	20:15:37:10
Q_2	Q	0.2 adequate	93 Apr 15.7 ±18.9	0.36 ±0.02	–0.078 ±0.006	+0.194 ±0.014	+0.297 ±0.017	15 ±0.077	197.86 +14.32	7.56 +4.30	158.76 +172.29	20:19:43:52 ■
	Q	0.1 adequate	93 May 2.1 ±13.0	0.37 ±0.03	-0.082 ±0.004	+0.185 ±0.034	+0.307 ±0.032	9 ±0.053	197.83 +16.59	8.67 +4.81	156.76 +178.27	20:19:43:33
T	S	0.3 robust	92 Dec 10.8 ±18.1	0.77 ±0.04	+0.272 ±0.028	+0.278 ±0.095	+0.660 ±0.031	15 ±0.155	166.75 +6.14	359.46 +0.26	165.79 +176.42	21:18:30:16
	S	0.2 robust	92 Dec 14.6 ±16.9	0.78 ±0.02	+0.274 ±0.026	+0.306 ±0.030	+0.665 ±0.021	11 ±0.135	167.39 +5.08	359.70 +0.39	166.54 +176.49	21:18:28:57
	u	0.6 adequate	92 Nov 5.1 ±37.8	0.68 ±0.09	–0.311 ±0.057	+0.270 ±0.168	+0.541 ±0.071	9 ±0.332	211.61 +11.44	357.28 –0.92	144.34 +175.69	21:18:10:27 o
	u	0.4 robust	92 Nov 9.4 ±26.8	0.78 ±0.06	–0.326 ±0.042	+0.368 ±0.060	+0.603 ±0.062	7 ±0.238	209.02 +8.74	357.55 –0.77	147.67 +175.80	21:18:08:41
	V^d	0.5 adequate	92 Sept 16.6 ±29.8	1.00 ±0.15	-0.612 ±0.123	+0.353 ±0.241	+0.703 ±0.136	10 ±0.302	221.23 +9.46	354.39 –2.60	132.96 +174.23	21:18:08:50
	V	0.3 robust	92 Sept 15.0 ±26.3	0.99 ±0.11	–0.604 ±0.109	+0.349 ±0.152	+0.696 ±0.094	5 ±0.178	221.02 +9.72	354.30 –2.66	133.07 +174.16	21:18:09:43
	W	0.6 adequate	92 Ott 21.3 ±18.1	1.77 ±0.16	-1.050 ±0.104	+0.755 ±0.204	+1.206 ±0.175	13 ±0.363	222.20 +7.62	356.41 –1.41	133.96 +175.35	21:17:56:54
	W	0.4 robust	92 Ott 8.0 ±13.9	1.61 ±0.10	–0.958 ±0.079	+0.628 ±0.179	+1.132 ±0.081	7 ±0.232	221.60 +8.64	355.63 –1.86	133.76 +174.99	21:18:09:25
u	w	0.3 adequate	92 Ott 16.0 ±8.4	0.89 ±0.03	–0.706 ±0.034	+0.284 ±0.022	+0.459 ±0.017	19 ±0.168	235.09 +12.50	356.09 –1.60	120.58 +175.21	21:22:00:09
	w	0.2 robust	92 Ott 7.3 ±6.4	0.87 ±0.02	–0.671 ±0.026	+0.271 ±0.017	+0.483 ±0.019	12 ±0.106	232.69 +12.66	355.58 –1.89	122.46 +174.96	21:22:01:18 ●
V	W	0.3 adequate	92 Dec 10.4 ±0.2	0.60 ±0.01	-0.349 ±0.001	+0.278 *0.010	+0.406 ±0.007	31[g] ±0.135	222.85 +9.11	359.44 +0.25	135.77 +176.41	22:04:23:30
	w	0.2 adequate	92 Dec 7.3 ±0.2	0.59 ±0.01	-0.344 ±0.001	+0.264 ±0.009	+0.402 ±0.006	23[g] ±0.104	222.88 +9.65	359.25 +0.15	135.49 +176.37	22:04:23:30 ●

[a] Angle between the fragment–Sun vector and the separation-velocity vector at the time of secondary-fragmentation event.
[b] Calculated as the angle subtended by the Jupiter-fragment vectors at perijove and at the time of secondary-fragmentation event.
[c] As observed at the Earth.
[d] Systematic trends in the residuals.
[e] Five-parameter solution: differential deceleration = 8.11 ± 0.98 units of 10^{-5} solar attraction.
[f] Five-parameter solution: differential deceleration = 8.75 ± 0.85 units of 10^{-5} solar attraction.
[g] Includes a pseudo-observation generated from the known impact time and location of the secondary fragment.
[h] Five-parameter solution: differential deceleration = 17.8 ± 2.2 units of 10^{-5} solar attraction.
[i] Based on Hubble Space Telescope observations only. When Q is involved, its position is assumed to coincide with that of Q_1.
[j] Five-parameter solution: differential deceleration = 18.6 ± 2.8 units of 10^{-5} solar attraction.
[k] Five-parameter solution: differential deceleration = 34.5+ 11.6 units of 10-s solar attraction.
[l] Five-parameter solution: differential deceleration = 32.0+ 5.7 units of 10-s solar attraction.
[m] Five-parameter solution: differential deceleration = 66.6+ 4.1 units of 10-s solar attraction.
[n] Five-parameter solution: differential deceleration = 55.0* 6.7 units of 10-s solar attraction.

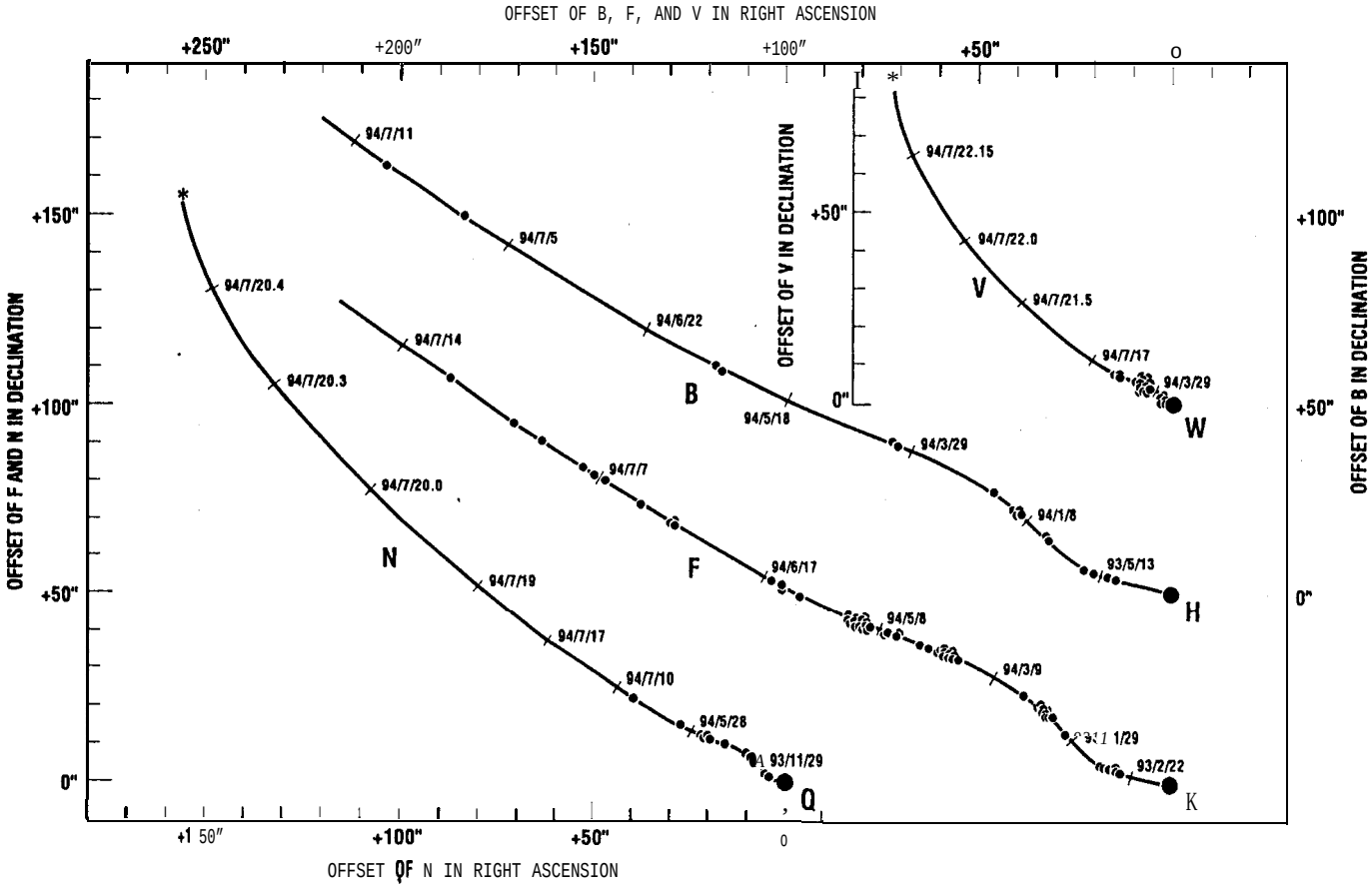

Fig. 1. Motions of daughter fragments relative to their parent fragments in projection onto the plane of the sky. The individual pairs are B relative to H, F relative to K, N relative to Q, and V relative to W. The large solid circles are the fixed locations of the parents, the dots are the offsets "daughter minus parent" from the employed astrometric observations, the asterisks on the trajectories of fragments N and V are the observed impact events used as pseudo-observations, and the curves are the best optimized dynamical solutions from Table 1. Note that the scales for the four pairs are shifted relative to each other.

When the tabulated value for the rejection cutoff is smaller than 0.2 arcsec, it represents the maximum residual of all the available observations, rounded off upward to the nearest multiple of 0.05 arcsec; the involved astrometric data are those from the HST or the best ground-based observations. The convergence of a solution is characterized as *robust*, when in the differential-correction procedure the absolute value of the iterated correction to each of the separation-velocity components can eventually be reduced to about 0.0001 m/s or less and the iterated correction to the time of separation to about 0.005 day or less. The convergence is described as *adequate*, when the absolute values of the respective corrections can be reduced to <0.0004 m/s and <0.05 day; and it is judged to be *weak*, when they fail to drop below ~ 0.001 m/s and ~ 0.1 day. When the correction values cannot be brought down even to these levels, it is concluded that such solutions have not converged and they are not listed in Table 1. Only two weakly converging solutions are tabulated. A symbol in the table's status column (identical with the symbol used in Fig. 4) indicates the solution that was selected as the most representative one among the scenarios considered for the given daughter fragment. Each such solution is employed in our further analysis (Sect. 5). The bullets and open circles refer to the 1992 breakup episodes with the bullets relating to what we believe are genuine secondary fragments. The open circles refer to tertiary fragments, the square identifies the only 1993 event detected, while the stars mark probable primary fragments.

Table 2 presents information on the scenarios for secondary-fragmentation events which were considered but failed to result in converging four-parameter or five-parameter solutions, or for which solutions were not attempted for important reasons. The individual columns yield the daughter fragment, the assumed parent fragment, the rejection cutoff employed, and a description of the difficulties encountered.

In the following, we describe and evaluate details on the results of our orbital analysis for the individual events of secondary fragmentation.

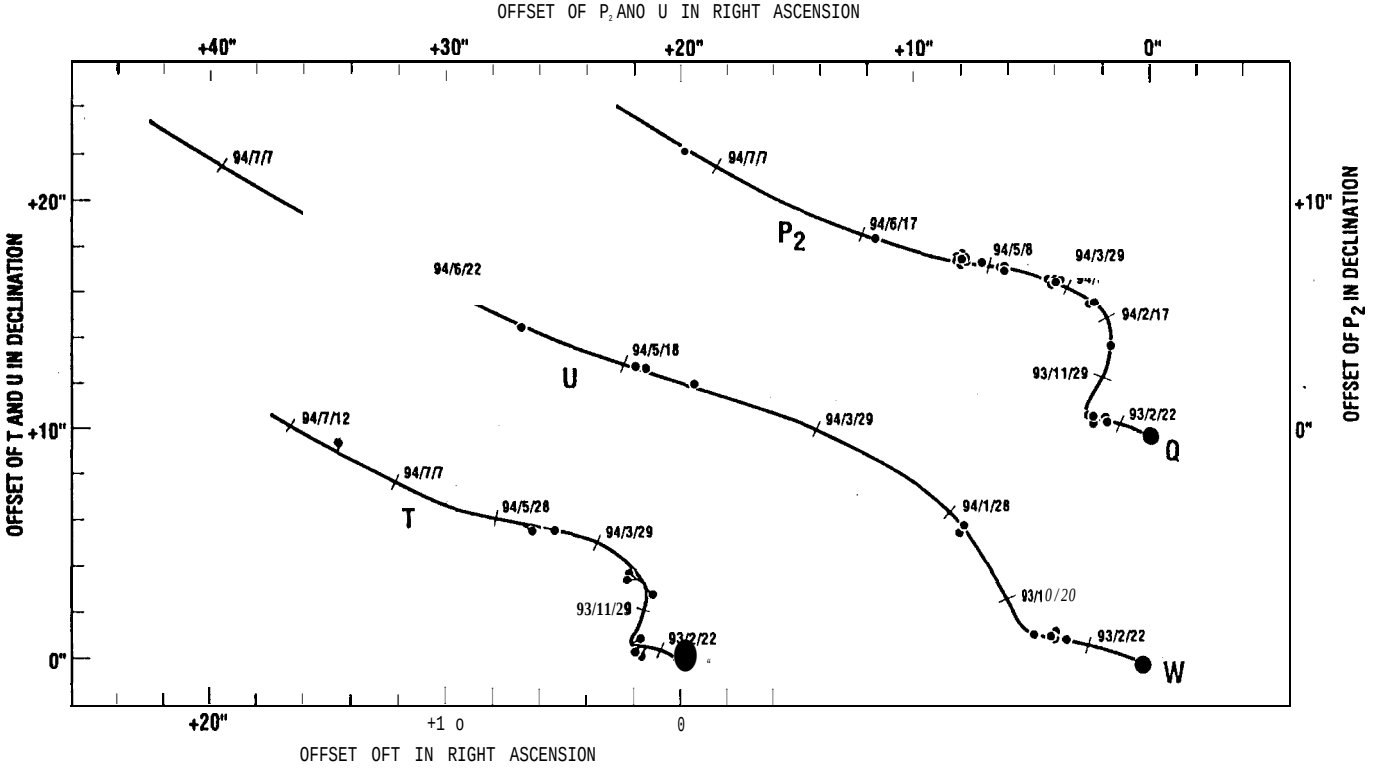

Fig. 2. Motions of daughter fragments relative to their parent fragments. The individual pairs are: P_2 relative to Q, T relative to U, and U relative to W. See the caption to Fig. 1 for more details.

4.1. Condensation A

We investigated the possibilities that A could have been derived fro-m C, E, or G but none of these scenarios was found to be acceptable.

Insurmountable convergence difficulties were encountered in searches for four-parameter solutions with C or E as the parent. Sets of three-parameter solutions indicate a broad minimum in the sum of squares of the residuals that is centered on Aug. 5 ± 29 days and July 23 ± 40 days when C and E, respectively, are assumed to have been the parent. The perijove time is within 1σ of the result for C and within 0.5σ for E. Also, the premise of A as a small fragment of C is hard to defend because the impacts of these two nuclei were rated to be comparable in magnitude both morphologically (Hammel *et a/.* 1995) and in terms of a peak near-infrared flux (Nicholson 1996).

The premise of G as the parent led to a converging four-parameter solution (a separation on August 18-20, 1992 with a velocity of ~ 1.6 m/s for the rejection cutoffs of 0.2–0.3 arcsec). However, the predicted impact time was too early by approximately 5 minutes, which for this fragment is considered unacceptable.

Because of the on-train position of this condensation (Sect. 7), it is argued that A is most probably a product of the progenitor's remnants separated in a breakup that was part of the initial disruption in July 1992.

4.2. Condensation B

This is one of the most difficult cases for identifying the parent fragment. Altogether, seven potential parents were under consideration: A, C, D, E, F, G, and H.

We soon dismissed the hypotheses that assumed the parent to be A, C, D, or E. Their common weakness was a strong systematic trend, in excess of 1 arcsec, in the residuals from the positional offsets in July 1994.

The premise of fragment F as the parent would make B a tertiary fragment (Sect. 4.5). With a rejection cutoff of 0.3 arcsec, the converging four-parameter solution (Table 1) left systematic residuals in the pre-conjunction 1993 offsets of at least 0.2 arcsec in both coordinates. In any case, this solution is invalidated by the predicted time of separation of fragment B from F which precedes the computed time of birth of fragment F (Table 1). Restricting the residuals to 0.2 arcsec would require that all pre-conjunction 1993 data points be discarded. Such solutions would clearly be inferior and they were not included in our search.

The assumption of fragment G as the parent resulted in a converging four-parameter solution (Table 1) that left systematic residuals of nearly 0.4 arcsec in the pre-conjunction 1993 offsets in declination. No attempt was therefore made to search for solutions constrained by a rejection cutoff tighter than 0.4 arcsec.

Table 2. Secondary-fragmentation scenarios for which four- and five-parameter solutions failed or were not attempted.

Fragment		Rejection Cut off (arcsec)	Description of difficulties encountered
Daughter	Parent		
A	C	0.3; 0.2	no convergence for four-parameter solutions; three-parameter solutions suggest that A probably separated from the progenitor's remnants in a breakup that was part of the initial disruption
	E	0.3; 0.2	no convergence for four parameter-solutions; three-parameter solutions suggest that A probably separated from the progenitor's remnants in a breakup that was part of the initial disruption
	G	0.3; 0.2	converging four-parameter solution yields an impact time that is inconsistent with observational evidence
B	A	0.4; 0.3	no convergence for four-parameter solution; three-parameter solution suggests T_{sep} < Jul 10; strong systematic trends in the residuals; when introduced, deceleration is poorly defined and negative
	c	0.4; 0.3	no convergence for four-parameter solution; three-parameter solution suggests T_{sep} < Jul 10; strong systematic trends in the residuals; when introduced, deceleration is poorly defined and negative
	D	0.4; 0.3	no convergence for four-parameter solution; three-parameter solution suggests T_{sep} < Jul 10; strong systematic trends in the residuals; when introduced, deceleration is poorly defined and near zero
	E	0.4; 0.3	no convergence for four-parameter solution; three-parameter solution suggests T_{sep} < Jul 10; strong systematic trends in the residuals; when introduced, deceleration is poorly defined and near zero
	F	<0.3	solutions not searched for, as all pre-conjunction 1993 data points would have to be discarded to satisfy this constraint
	G	<0.4	solutions not searched for, as all pre-conjunction 1993 data points would have to be discarded to satisfy this constraint
D	E	0.2	no convergence for four-parameter solution; three-parameter solution suggests T_{sep} < Jul 10; predicted impact time for D grossly inconsistent with observational evidence
	G	0.3; 0.2	no convergence for four-parameter solutions; three-parameter solutions suggest T_{sep} < Jul 10; predicted impact time for D grossly inconsistent with observational evidence
F	G	<0.3	solution not searched for, as all pre-conjunction 1993 data points would have to be discarded to satisfy this constraint
G_2	G	.....	weakly converging four-parameter solution yields T_{sep} = 1992 Aug 5 ± 120 days and a separation separation velocity that is indeterminate; no convergence for five-parameter solution
M	N	. ...!	no convergence for four-parameter solution; three-parameter solution shows systematic trends in the residuals
T	S	0.3	five-parameter solution shows the deceleration to be essentially indeterminate
	u	0.6	no convergence for five-parameter solution
	v	0.6	no convergence for four-parameter solution; three-parameter solution suggests T_{sep} < Jul 10; predicted impact time grossly inconsistent with observational evidence; when introduced, the deceleration is indeterminate
U	V	0.3; 0.2	both four- and three-parameter solutions consistently yield T_{sep} < Jul 10

Somewhat surprisingly, the assumption of fragment H as the parent was the only one that offered formally satisfactory four-parameter solutions. Their convergence was robust for all three assumed values of the rejection cutoff, 0.4, 0.3, and 0.2 arcsec (Table 1), and there were no systematic trends in the residuals. When a deceleration was introduced as a parameter, its value came out to be essentially zero and the offset residuals were not improved. The dynamical parameters are quite consistent: the predicted time of separation on 1992 August 3–12, with a formal error of less than ±10 days, and the separation velocity between 1.5 and 1.8 m/s, with a formal error of less than ±0.2 m/s. Although this rate of separation is relatively high (Sect. 6), we conclude that H is indeed the best candidate for fragment B's parent and that this separation occurred four to five weeks after perijove.

In our runs, the predicted time of impact is never earlier than about 2:59 UTC (at the Earth) on July 17, 1994. For the three best solutions, with H as the parent, the impact times are between 3:01 and 3:05 UTC. This is consistent within a $\sim 2\sigma$ uncertainty with Hammel *et al.*'s (1995) result of 2:56+3 minutes from measurement of the impact site. A detection of the impact of B was reported by de Pater *et al,* (1994) between 2:56 and 3:13 UTC; in Table 1 of Paper 2 this is tentatively identified with the main event. However, this duration is much longer than the 10 minutes recorded for the main event of fragment R, a more massive object, with the same telescope several days later (Graham et *al.* 1995). Unfortunately, the recording chart of event B has a gap from 2:59 to 3:09 (de Pater 1997), so that its temporal profile cannot be ascertained. If fragment B disintegrated entirely into a dust-particle stream before entering the jovian atmosphere and de Pater *et al.*'s (1994) observations refer to the stream's atmospheric entry, our predicted time is in very good agreement with the reported timing, If the observation refers to the main event, the impact time from our adopted solution (Table 1) is 11-12 minutes too late. Circumstantial evidence for an early disintegration of fragment B is provided by Beebe (1996), who concluded that the dark material in site B was located higher in the atmosphere than the other dark features.

The fragments from K on have not been tested as potential parents of B because unrealistically high separation velocities of ~ 2 *m/s* or more would be required.

4.3. Condensation C

In spite of its insignificant (<1 arcsec) positional deviation from the train (Sect. 7), this fragment's status has been unclear. Since the prominence of the C impact event was judged to be on a par with those of the on-train fragments A, E, and H (Hammel *et al.* 1995), it appears that the *a priori* chance for C being a product of secondary fragmentation is fairly remote. A study of C as such can nevertheless be justified by referring to Nicholson (1996) who classified the C impact as small, one category below E and H and two categories below G.

These three fragments, E, G, and H, were considered as possible parents of C and a search for plausible scenarios was initiated. Converging and fairly satisfactory solutions were obtained in all three cases, as shown in Table 1. The best agreement with the adopted time of impact (Paper 2), which was based primarily on Takeuchi *et al.*'s (1995) near-infrared observations of the second precursor, is provided on the assumption that H was the parent; the discrepancy in the predicted time of impact is then reduced to less than 30 seconds. However, from the evidence presented in Sect. 7, we prefer to consider the history of C to be similar to that of A; fragment C may have been one of the last primary fragments that separated from the progenitor's remnants in July 1992.

4.4. Condensation D

The history of this fragment resembles that of C both in that its status has been somewhat unclear and that it shows no significant deviation from the nuclear train, Also, Nicholson (1996) rated the impact phenomena due to these two fragments as comparable in terms of the peak near-infrared flux, Unlike C, however, the D impact event was classified by Hammel *et al.* (1995) to be in the same category as the impact phenomena of B, N, and Q_2, all of which belong to the group of the off-train condensations. We investigated the hypotheses of D having been derived *from* E, G, or H.

Considerable convergence difficulties were encountered in our attempts to find a solution for D as a daughter fragment of E (Table 2). The best result of many hundreds of iterations, made during our experimentation with the rejection cutoff and the variation steps, was a weakly converging solution listed in Table 1. Although the predicted time of impact is in excellent agreement with the value adopted in Paper 2, the weak convergence offers very little confidence in this solution. Similarly unsuccessful were our efforts to come up with a meaningful scenario with *G* as the parent fragment (Table 2). In this *case,* the predicted impact time was always grossly inconsistent with that adopted in Paper 2. A common trait of our attempts to derive quasi-optimized three-parameter solutions for either E or G as the parent was an early time of separation, near or before July 10, 1992, suggesting that D was probably a primary fragment.

As in the case of C, the premise of H as the parent of D led to converging four-parameter solutions for the rejection cutoff values of 0.4, 0.3, and 0.2 (Table 1), but the predicted impact time differed from the adopted value by 4-5 minutes. This result strengthened our conviction that the history of D was most probably similar to that of A and/or C, with perhaps an even greater chance that it was the last among the primary fragments to break away from the progenitor's remnants in July 1992.

4.5. Condensation F

Three potential parent fragments, G, H, and K, were tested for F. Of these, the solutions obtained on the assumptions that either of the first two fragments was the parent were rather unsatisfactory because they all left systematic trends in the offset residuals from the preconjunction observations. The G solutions could not accommodate the offsets measured on the HST images from July 1, 1993 to better than ~ 0.3 arcsec. On the other hand, the H solutions, while fitting the July 1 offsets satisfactorily, left unacceptably large systematic residuals of up to 0.6 arcsec from the early 1993 observations which had to be ignored. No improvement was achieved when the deceleration was included as an additional solution parameter.

The assumption of fragment K as the parent led to different results. Our search for a successful four-parameter solution failed miserably since the July 1994 offsets could not be fit and left systematic offset residuals in excess of 0.5 arcsec. The situation became much more encouraging when a deceleration was introduced as an additional parameter , The systematic trends in the residuals disappeared and the predicted time of impact was moved back by ~ 13 minutes. Even though the derived deceleration is relatively small (Table 1), it is very well determined with a signal-to-noise ratio of 8 to 10.

4.6. Condensation G2

This fragment was first detected by Jewitt and Trentham (1994) on May 7, 1994 at a separation distance of about 5 arcsec from G. Subsequently,' G_2 was also identified on the HST images from March 29 and May 17 (Nell and Smith 1994) as well as on ground-based images taken by D. Tholen, R. Whiteley, and T. Kim on May 5, 6, and 14 (Tholen 1994). A weakly converging solution based on the six observations yielded essentially meaningless results that are not included in Table 1 (a separation on 1992 August 5 ± 120 days with a velocity of 0.5 ± 0.5 m/s). Other attempted solutions failed to converge, including one with a deceleration introduced as a parameter.

4.7'. *Condensation J*

The candidate parent fragments considered were K, L, and N. In the first two scenarios J would be a secondary fragment, while in the third scenario, a tertiary fragment.

This is one of two condensations that were observed only by Jewitt *et al.* (1993) between March 27 and July 17, 1993. Its possible detection on an image taken by D. Tholen with the 224-cm reflector at Mauna Kea on 1993 Dec. 14.648 UTC and measured by Scotti (1993) is ruled out, as the offsets leave residuals of 3 arcsec or more regardless of the identity of the parent fragment.

The best solutions for the three scenarios are listed in Table 1, The predicted time of impact is not a criterion, because no evidence on the impact phenomena is available. Nominally, the superior solution is offered by the scenario with N as the parent, which yields the least RMS residual. This is our preferred scenario, but we notice (Sect. 4.9) that the separation of J from N must have occurred immediately after N had separated from Q.

4.8. *Condensation M*

The second of the two condensations detected only by Jewitt *et al. (1993)* in March-July of 1993, this fragment was considered to have separated either from Q or P. The predicted impact time in the latter scenario would provide a fairly good match to the apparently observed main event (Table 1 of Paper 2). Unfortunately, this option is invalidated, because it implies with fairly high probability the separation of M from P before the separation of P from Q (Sect. 4.10). Reluctantly, we adopt Q as the direct parent of fragment M, even though the predicted impact time is off by more than 1 hour.

4.9. Condensation N

This is the only secondary fragment whose jovian impact was observed with an instrument onboard the Galileo spacecraft. Chapman *et al. (1995)* reported that the luminous event, detected by the Solid State Imaging camera, lasted from 10:29:17 to 10:29:32 UTC on July 20, 1994 and that the rise time of the initial sharp flash was ~3 seconds. This constrains the impact to a period of time from 10:29:17 to 10:29:20 UTC; the two boundaries were adopted for the impact time, respectively, by Nicholson (1996) and in Paper 2.

The only parent candidate considered for N was fragment Q. We were unable to find a converging four-parameter solution based on the offsets from the existing observations. However, we employed the accurately known impact time of fragment N to generate a pseudo-observation: we calculated the astrometric positions for N and Q (actually Q_1) from their respective orbital elements (Paper 2) at the time of impact, 1994 July 20.437 UTC. Then we combined these derived offsets in right ascension and declination with the offsets calculated from the available observations and searched for a strengthened solution. The incorporation of the pseudo-observation into the optimization procedure had an extremely beneficial effect on the determinacy of the separation parameters, as seen from Table 1.

4.10, *Condensation P (later* P_2 *or* P_{2a}*)*

It has already been established in Paper 1 that this fragment had separated from Q (see also Sekanina 1996). In the present study we started by searching for a four-parameter solution, using the offsets of P_2 on two dates (July 1, 1993 and January 27, 1994) and P_{2a} on one date (March 30, 1994) relative to Q_1, available from measures on the HST images. The result was disappointing; the converging solution yielded a mean residual of +0.17 arcsec, about five times the typical error of positional measurement on the HST images taken in the Planetary Camera mode. The fit was improved considerably, with the mean residual reduced to ±0.038 arcsec, when the deceleration was introduced as an additional parameter (Table 1). Nevertheless, this improvement was largely cosmetic, because the fact that P separated from Q, not P_2 from Q_1, remained unaccommodated. Strictly, one should begin with modelling the motion of the unknown barycenter of P_2 and P_1 relative to the unknown barycenter of Q_1 and Q_2. Since this cannot be done in practice, the problem

is to some extent rectified by considering only the high-resolution data reported by the ground-based observers, who in most cases measured only a single P fragment and a single Q fragment,

This approach, while by no means perfect, led to converging four-parameter solutions for the rejection cutoff of both 0.3 and 0.2 arcsec. As is evident from Table 1, the introduction of a deceleration improved the result somewhat by accommodating a few more data points and modestly reducing the mean residuals. Since the signal-to-noise ratio of the deceleration came out to be as high as 8, we selected this to be our preferred solution.

4.11. Condensation P_1

Two obvious candidates for the parent were fragments P and Q. The early runs indicated that' no four-parameter solution could successfully match the offsets from either presumed parent. This conclusion was reached independently of whether the data came from the HST or the ground-based observations.

The solutions based on the premise that fragment Q was the direct parent suffered from the lack of knowledge of the barycenter of Q_1 and Q_2 just as did the solutions for P. The ground-based observations yielded, regardless of the applied rejection cutoff, very late separation times (Table 1) and predicted for July 1, 1993 separations that were grossly inconsistent (in excess of 1.5 arcsec) with the separation reported from the HST observation. This could not be an effect of Q_2, which at the time was only -0.3 arcsec away from Q_1. When only the HST offsets were employed, the problem of the barycenter correction again came to the forefront. Strong systematic residuals left in virtually all instances in which P_1 was reported from the ground illustrate these difficulties.

By contrast, we found the five-parameter solution based on the HST observations alone and on the assumption of the parent being identical with P to be very attractive, as it fit 13 separations of P_1 from P_2 reported from the ground. Unfortunately, the run that combined the ground-based and the HST entries did not offer anything beyond a weakly converging solution (Table 1). Under the circumstances, the preferred solution remains the one based solely on the HST data.

4.12. Condensation P_{2b}

This condensation was detected only on the HST images taken on March 30, 1994 (Weaver *et* al. 1995). Using his digital deconvolution technique, Sekanina (1995) was able to resolve two point sources near the general location of P_{2b}, with the source 2 (Fig. 3 of Sekanina 1995) as the prime candidate. He also was able to detect the same fragment as the source 2 in the digitized image of P_2 from January 24, 1994 (Fig. 2 of the same paper). Still, this information is insufficient to examine adequately the relative motion of P_{2b}. From a set of three-parameter solutions, we find the nominal time of separation to have been early December 1993. However, the separation velocity is indeterminate and the solution is based on the assumption of no deceleration, for which we cannot solve. The several months preceding the nominal date are more probable candidates for the true separation time.

4.13. *Condensation* Q_2

There is no doubt about the parent for this condensation, detected only ~0.3 arcsec from Q_1 on the HST image from July 1, 1993 (Weaver *et al.* 1995). The two presented solutions extend the previous solution (Sekanina 1996). We ascertained that the HST-based data could be combined with the data from several high-resolution ground-based observations to provide what we consider our best four-parameter solution. We also introduced a deceleration as a solution parameter but found it to be very small and poorly determined.

4.14. *Condensation T*

Altogether we considered four candidates for this condensation's parent — S, U, V, and W. Since T always projected onto the tail of S, we examined whether it could have been derived from S. The search for a solution based on this premise was entirely unsuccessful with strong systematic residuals (in excess of 1 arcsec) in both right ascension and declination throughout the period of April–July 1994. When the deceleration was added to the list of parameters, it was poorly determined and the quality of fit was not improved.

By contrast, fragment U turned out to be an excellent candidate, except that simultaneous measurements of T and U were much too infrequent. In order to include as many data as possible, we had to relax our standard rejection cutoff of 0.2–0.3 arcsec by a factor of two. Even so, we ended up with fewer than 10 offset pairs and have to contend with a fairly high formal error of the separation time, We see no systematic trends in the residuals. When the deceleration was solved for, the solution failed to converge.

Fragment V could readily be discounted as a parent of T for two reasons. The residuals were entirely unacceptable with large systematic trends in both right ascension and declination. In addition, the predicted separation time, in mid-September 1992, violates the basic rule for the tertiary fragments: T would have separated from V long before V separated from W (Sect. 4.16).

The solutions with fragment Was the presumed parent of T encountered similar difficulties as the solutions with V, showing systematic residuals in both right ascension and declination.

Fragment U remains the only acceptable candidate for the parent of T.

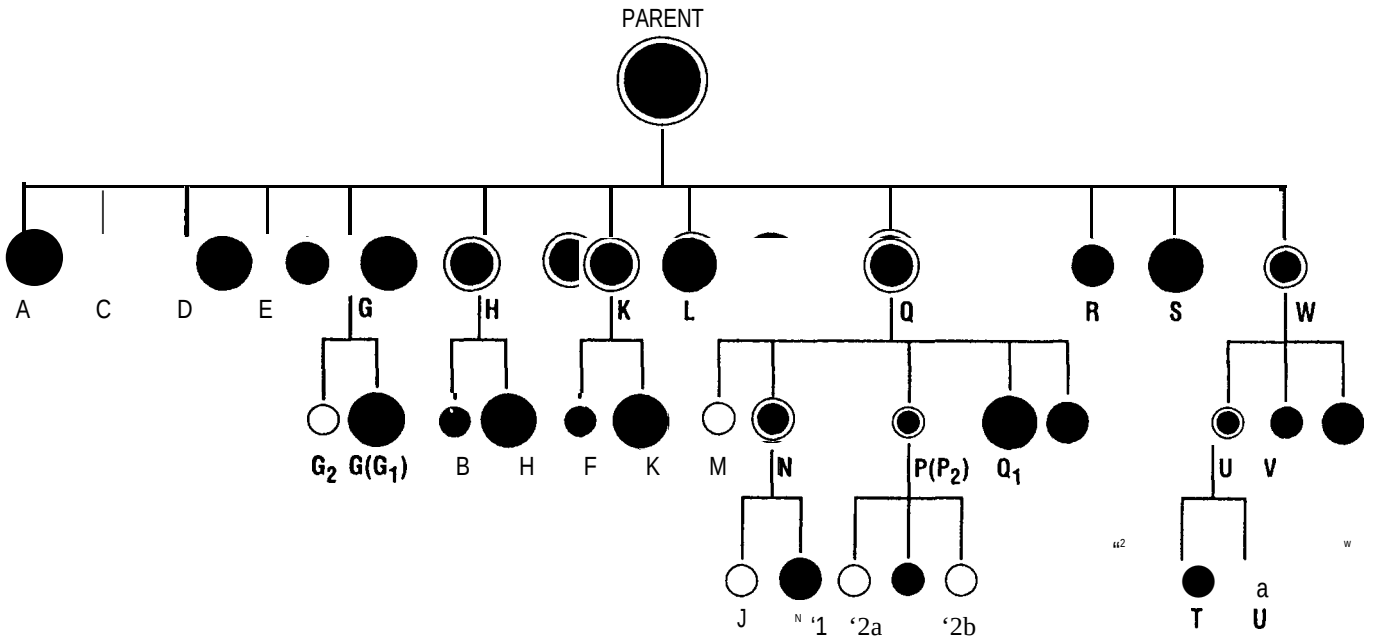

Fig. *3.* Hierarchy of nuclear fragmentation. The size of the symbols crudely characterizes the degree of prominence of the various fragments and their impact phenomena. Solid and open symbols refer, respectively, to the observed fragments that remained visible until collision with Jupiter and to those that disappeared earlier. Circled symbols refer to the nucleus of the progenitor and to the primary and the secondary fragments that began to break up before the comet's discovery.

4.15. Condensation U

We considered only two fragments, V and W, as plausible candidates for the parent of U. All attempted solutions with V as the presumed parent pointed consistently to a separation time before July 10, 1992 (Table 2) and were therefore rejected. On the other hand, the solutions based on the assumption that fragment W was the parent were quite satisfactory and did not require the inclusion of the deceleration among the parameters. The predicted time of separation of fragment U from W is approximately one month before the predicted time of separation of fragment T from U.

4.16. Condensation V

Here we have another case, where the parent, this time fragment W, appears to be undisputed. We were able to find a four-parameter solution that offered an excellent fit to more than 30 offset pairs. Nevertheless, the time of impact predicted by this solution differed from the time derived from the observation of the first precursor (Nicholson 1996; Paper 2) by -2.5 minutes and we looked for ways to refine the result. The known time of impact allowed us to construct a pseudo-observation for this instant, following the same procedure as in the case of condensation N (Sect. 4.9). Accordingly, we were able to come up with improved solutions (Table 1) even though the differences between these and the starting four-parameter solution (not listed in Table 1) are relatively minor in terms of both the separation time and the separation velocity. There was no need to introduce a deceleration.

4.17. Summary of findings

The case-by-case analysis of the discrete breakup events provides us with information necessary to establish a probable hierarchy of nuclear fragmentation of comet Shoemaker-Levy 9, which we present schematically in Fig. 3. In simple terms, there are essentially three kinds of fragments — primary, secondary, and tertiary.

As primary we classify the 12 on-train fragments that consist of the nine nuclei not examined here plus the three nuclei that were subjects of Sects. 4.1, 4.3, and 4.4. The complete list is: A, C, D, E, G, H, K, L, Q (later Q_1), R, S, and W. All we can say about them at this point is that (i) they were products of an early fragmentation phase of the progenitor comet shortly after its perijove passage on 7 July 1992 and, in any event, they existed as independent objects by the end of that month; and (ii) the separation times for the three of them examined here — A, C, and D — could at best be only barely distinguished from the time

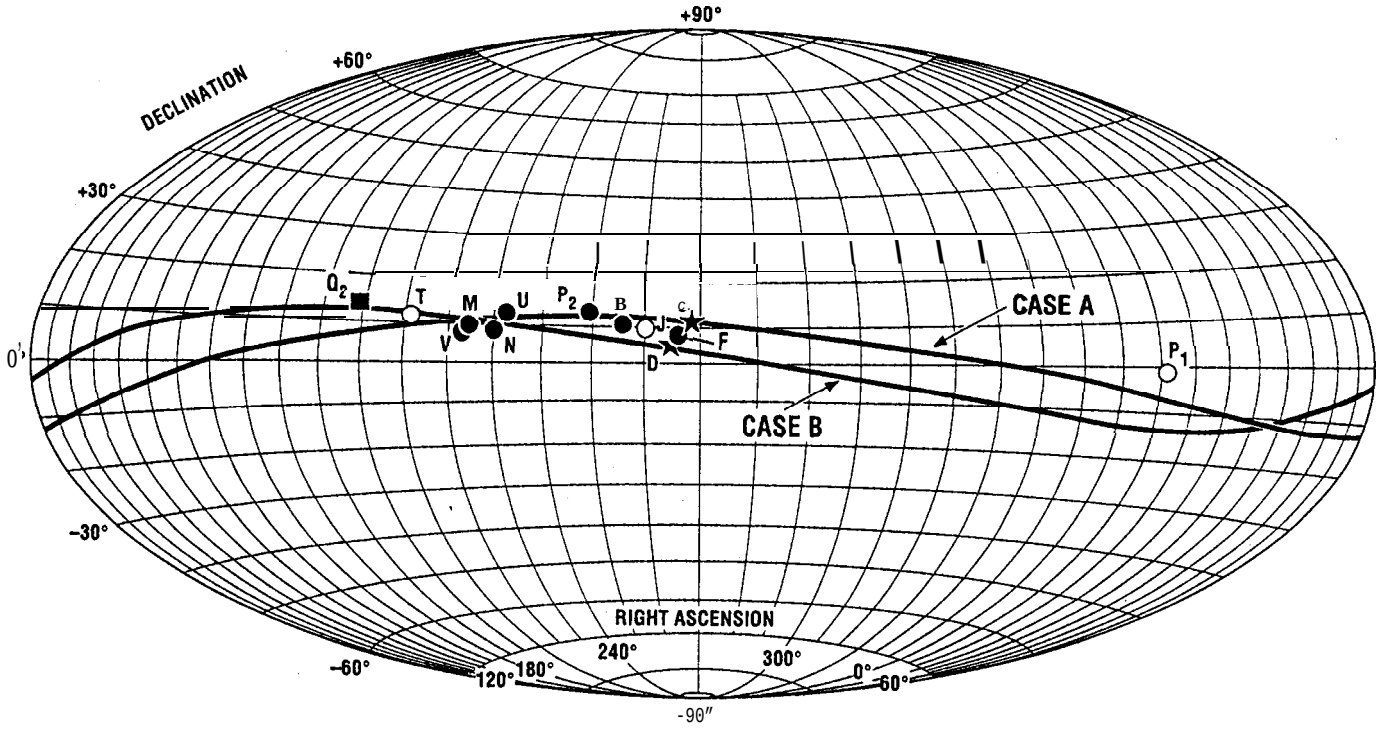

Fig. **4.** Right ascensions and declinations for the selected separation-velocity vectors of the 13 fragments from Table 1. Each entry is marked by the presumed daughter fragment's letter and by the symbol from the table's Status column. (Note that C and D are in fact the primary fragments.) The two curves are the great circles fit, respectively, through all the 11 points that refer to the secondary and tertiary fragments (Case A in Table 3) and through the eight points that depict only the secondary fragments (Case B). The coordinates of the corresponding rotation poles are listed in Table 3.

of perijove by the techniques employed. We will return to the topic of the early phase of the fragmentation process in Sects. 7 and 8.

Among the 13 off-train fragments examined, we identify nine as secondary: B, F, G_2, M, N, P (later P_2 or P_{2a}), Q_2, U, and V; and four as tertiary: J, P_1, P_{2b}, and T. Available information on two of these — G_2 and P_{2b} — is too incomplete to offer a meaningful dynamical solution, even though the identities of their parents are not an issue. Interestingly, all 13 secondary and tertiary fragments were derived from only five primary fragments (G, H, K, Q, and W). Eight observed fragments had Q as their common parent.

In the scenario that we propose here as the most likely, the first event of secondary fragmentation took place in early August 1992 when B separated from H. About a week later N broke off from Q and immediately J from N. In the last days of August F separated from K and M from Q. In early October fragment U split off from W and in early November P from Q and T from U. It is also probable that during November P_1 separated from P, which became P_2. Fragment V broke off from W in early December 1992 and Q_2 from Q (which became Q_1) some four months or so later, during April 1993. The time of separation of G_2 from G is nearly entirely indeterminate while P_{2b} apparently broke off from P_2 (which became P_{2a}) during the second half of 1993.

The temporal distribution of the 11 events of secondary fragmentation for which adequate information is available is thus strongly nonuniform. Nominally (disregarding the errors involved), five of the 11 episodes are calculated to have occurred in August 1992, within eight weeks following the perijove passage. An additional five separations are found to have taken place in a two-month period between early October and early December 1992, and one in April 1993. The overall pattern suggests that the fragmentation rate was decreasing with time, perhaps quasi-exponentially.

The derived separation-velocity vectors are also distributed very nonuniformly both in direction and in magnitude. Figure 4 displays, in right ascension and declination, the distribution of orientations of the separation-velocity vectors for the 13 fragments listed in Table 1. The figure demonstrates that the vectors are arranged essentially along a great circle, with an average scatter of not more than a few degrees. One of the most fundamental results of our study, this effect is thoroughly examined in Sect. 5.

The velocities of separation for the 13 fragments are found to have ranged from 0.36 m/s for Q_2 up to 1.7 m/s

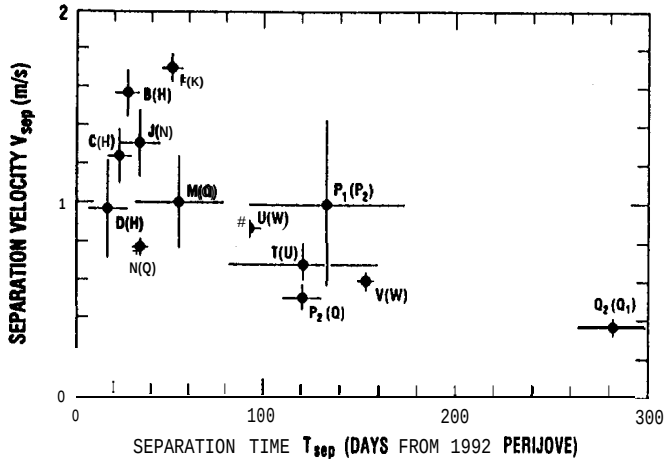

Fig. 5. The correlation between the separation time and the separation velocity from the selected solutions for the 13 events of discrete fragmentation listed in Table 1. The symbols used are those introduced in the t able's Status column. Each individual entry is identified by the daughter fragment, with the parent fragment parenthesized.

for F. An average for the 11 secondary and tertiary fragments in Table 1 is 0,92 m/s. There is a correlation between the separation velocity and the separation time, as illustrated in Fig, 5. The significance of this correlation is addressed in Sect. 6.

The role of the differential deceleration in the relative motions of the fragments involves two major issues: (i) an explanation of its absence for most fragments and (ii) an interpretation of its meaning in the *cases* of P_1, P_2, and F, for which its introduction was necessary.

The first significant point to notice is that PI, P_2, and F are all among the fragments that displayed no detectable impact phenomena (Table 1 of Paper 2), This negative evidence suggests that virtually the entire mass of these condensations arrived at Jupiter in the form of highly dispersed streams of particulate material.

On the other hand, analysis of the HST digital maps from January and March 1994 indicates the presence of objects of up to ~2 km in diameter in condensations F and P_2 and objects of up to ~1 km in diameter in condensation PI (Sekanina 1995). In addition, the products of a secondary-fragmentation event were always two distinct condensations, not an elongated nebulosity. This evidence testifies to the presence of one dominant mass in each component at least at separation and for a limited period of time subsequent to it. The diffuse appearance of the condensations suggests that much of the involved dust population was released during the episode. Otherwise, one would have to postulate a bimodal velocity distribution in the parent condensation, a premise with no physical or dynamical rationale and virtually impossible to defend.

The only way to reconcile this seemingly contradictory evidence from the early and the late stages of evolution for fragments PI, P_2, or F is to accept that they were subjected to *progressive* fragmentation, gradually disintegrating into ever smaller particulate as time went by. Needless to say, this scenario does not apply indiscriminately to every single fragment, as documented by a great variety of the observed impact phenomena.

The plausibility of the proposed hypothesis of progressive fragmentation can be demonstrated by inspecting the imaging sequences of some of the fragments. Perhaps the most compelling example is that of PI, the fragment whose motion was subjected to the most conspicuous deceleration. A series of its HST images, reproduced by Weaver *et al.* (1995) in their Fig. 2, clearly shows the gradual change in the fragment's appearance, from a relatively compact condensation as late as January 1994 to an elongated, ever expanding wisp of material in the period of March-May and, eventually, to its disappearance in June. The important aspect of this process is the progressive loss of condensation, so that the nebulosity's "core" becomes increasingly illusory and its bisection difficult to impossible. What happens, in fact, is that even if there are fairly massive subfragments buried in the cloud of debris, they are optically so insignificant that the measurer has no choice but to bisect the nebulosity's centroid, which is determined entirely by the distribution and dynamics of dust particles of the prevalent size, even if, say, 10-meter-sized or larger objects are present. If optically dominant particles are small enough to be detectably affected by solar radiation pressure (<<50 cm in diameter at an assumed bulk density of 0.2 g/cm^3), then: (i) the majority of condensations, for which the brightness distribution in the innermost region remained dominated until (or almost until) the arrival at Jupiter by a single large mass or a compact aggregate of large boulders, is characterized by the absence of a deceleration and (ii) the brightness distribution near the center of P_1, P_2, and F apparently was, for some time before impact, dominated by particulate debris subjected to detectable effects of solar radiation pressure, which are described by the derived deceleration; the prevalent particle diameter is calculated to have amounted to ~7 cm for F, ~3 cm for P_2, and ~1 cm for P_1.

One issue remains to be addressed: the concept of progressive fragmentation implies that the deceleration must have increased with time, so that the solutions in 'Table 1 offer for these three fragments only "effective" deceleration values, which are higher than the intrinsic decelerations during the early phase of each fragment's evolution and lower (possibly much lower) than those during the final phase. From experience with the nongravitational terms in the equations of motion of comets, it is well known that the nongravitational parameters are determined primarily by the integrated effect of the force (regardless of its physical nature) and are largely insensitive to the force's temporal variations (e.g., Sekanina 1993). This is to be expected whenever one tries to determine a dynamical quantity from its second integral (in this case, positional

offsets). Thus, the apparent success of the five-parameter solutions (which force a *constant* deceleration) for P_1, P_2, and F is not surprising and the need to incorporate in these cases the deceleration among the dynamical parameters is not inconsistent with the evidence of a relatively massive, gravitationally dominant nucleus at the time of separation from the parent fragment and for a limited period of time afterwards.

5. Distribution of separation-velocity vectors for secondary fragments originating in the discrete events

We submit that the peculiar distribution of the separation-velocity vectors in Fig. 4 can only be interpreted as a product of the approximately conserved angular momentum of the progenitor comet at the time of initial disruption. Each daughter fragment is envisaged as having been "launched" tangentially from its parent fragment with a rotational speed that slightly exceeded the velocity of escape. The applied centripetal tension, assisted by potentially significant thermal stresses (Sect. 8) was apparently sufficient to spin off, from the parent fragment, one or more subfragments along planes of structural weakness, thus determining the size and shape of the resulting daughter fragments. Even if the spin rate did not change significantly following the progenitor comet's initial disruption, the rotation rate could easily exceed the critical escape limit from a primary fragment. Indeed, while the maximum dimension of primary fragments should be similar to that of the progenitor, yielding a rivalling rotation velocity, their individual masses were smaller, which necessarily implied a lower velocity of escape from the fragment's surface, compared with that from the progenitor's surface. For example, it can be shown that if the original comet should have split into 10 pancake-shaped fragments, the escape velocity from these fragments could drop to values as low as 0.4 the escape limit from the progenitor.

If the angular momentum of the progenitor cornet had approximately been conserved during its disruption into the primary fragments, this should be reflected in the vectorial distribution of separation velocities for the secondary fragments. In particular, the great circle fit to a set of separation-velocity vectors in Fig. 4 should identify the progenitor's equatorial plane at the time of initial disruption. Expressing the directions of the separation-velocity vectors in terms of the right ascension α and declination δ, the equation of this equatorial plane is

$$A_{\rm rot} \cos \alpha + B_{\rm rot} \sin \alpha + \tan \delta = \mathrm{O}, \qquad (1)$$

where $A_{\rm rot}$ and $B_{\rm rot}$ are constants defined by the right ascension $\alpha_{\rm rot}$ and declination $\delta_{\rm rot}$ of the progenitor comet's "northern" rotation pole (from which the nucleus is seen to spin counterclockwise) at the time of initial disruption:

$$A_{\rm rot} = \cos \alpha_{\rm rot} \cot \delta_{\rm rot}, B_{\rm rot} = \sin \alpha_{\rm rot} \cot \delta_{\rm rot}. \qquad (2)$$

The solution is ambiguous, because the coordinates of the "southern" pole yield the same values of $A_{\rm rot}$ and $B_{\rm rot}$.

In practice, these constants are determined by a least-squares optimization procedure from the distribution of the separation-velocity vectors (Sect. 6). The ambiguity is settled by an additional constraint, provided in Sect. 7 by the condition that the nuclear dimensions of the progenitor comet not exceed a certain limit. It turns out that only one sense of rotation satisfies this condition. If the unit rotation vector consistent with this sense is $\omega_{\rm rot}$, the unit separation vector $r_{\rm sep}$ is defined by a cross product

$$r_{\rm sep} = \mu \, (V_{\rm sep} \times \omega_{\rm rot}), \qquad (3)$$

where μ is a normalization constant ($\mu > \mathrm{O}$) and $V_{\rm sep}$ *is* the separation-velocity vector. Calling $r_\odot$ the fragment-Sun vector at the time of separation, we find from the dot product $(r_{\rm sep}, r_\odot)$ calculated for the 11 events involving the secondary and tertiary fragments that the locations of all separation points, except for PI, were (somewhat counterintuitively) on the antisolar side of the parents,

The angle γ that is subtended by the fragment-Sun and separation-velocity vectors is given by a dot product

$$\cos \gamma = \frac{r_\odot \cdot V_{\rm sep}}{\|r_\odot\| \cdot \|V_{\rm sep}\|} \qquad (4)$$

and listed in Table 1. On the antisolar side, $\gamma > 90°$ for the separation-point locations between sunset and midnight, while $\gamma < 90°$ for the locations between midnight and sunrise. On the sunlit side, the separation occurs before noon when $\gamma < 90°$ but in the afternoon when $\gamma > 90°$.

From Table 1 the angle γ is found to have varied from 12° for P_1 to 159° for Q_2. Of the 11 secondary and tertiary fragments in the table, nine separated from the parent before local midnight and only two (F in addition to P_1) after midnight. Four of these fragments have the angle confined to the interval 70–1 10°. In the context of the model formulated on the basis of our new results, the implications of the separation of the fragments from the antisolar side of the parent fragments are addressed in Sect. 8.

Once the progenitor's unit rotation vector has been established, we proceed to calculate the two Eulerian angles that define the orientation of the comet's jovicentric orbit plane at the time of initial disruption relative to its equatorial plane: the obliquity I and the argument Φ of the subjovian meridian at perijove (Fig. 6).

The coordinates $\alpha_{\rm jov}, \delta_{\rm jov}$, which describe the unit vector $\Omega_{\rm jov}$ pointing from the progenitor comet t o Jupiter's center at the time of perijove, can closely be approximated by the coordinates of the planet as seen from fragment K. Similarly, the coordinates $\alpha_{\rm orb}, \delta_{\rm orb}$, which describe the unit vector $\omega_{\rm orb}$ normal to the progenitor's orbit plane at the time of initial disruption, can be approximated by the coordinates for the northern orbit pole of fragment Ii at perijove. This approximation is accurate to a small fraction of 1°, which is superior to the determination of the

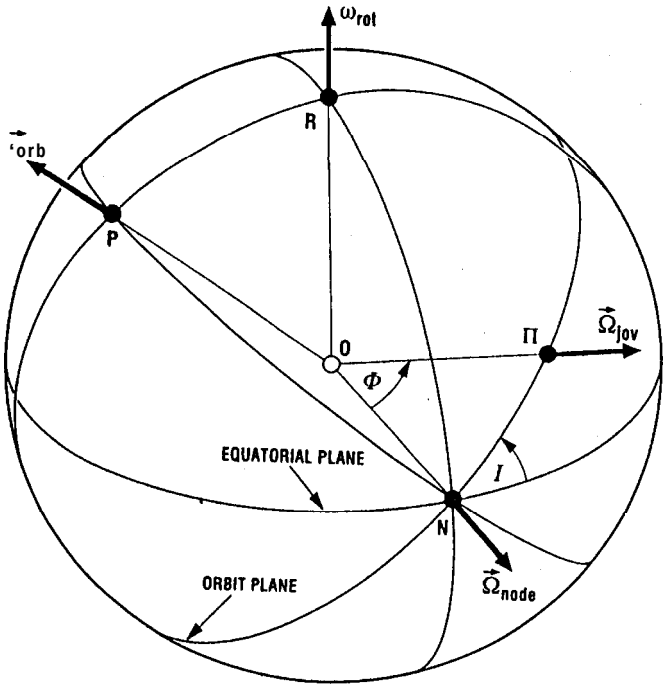

Fig. 6. Orientation of the equatorial and jovicentric orbit planes on a spinning comet and the definition of the rotation parameters. The point O is the nucleus center, P the northern orbit pole, R the northern pole of rotation, N the ascending node of the orbit plane on the equatorial plane (i. e., the comet's vernal equinox), and Π the subjovian point at perijove. Angle I is the obliquity of the orbit plane to the equatorial plane and Φ the argument of the subjovian meridian at perijove. The four corresponding umt vectors are ω_{orb}, ω_{rot}, Ω_{node}, and Ω_{jov}.

rotation pole (Sect. 6). The equation of the orbit plane at the time of initial disruption is

$$A_{orb} \cos \alpha + B_{orb} \sin \alpha + \tan \delta = 0, \quad (5)$$

where, in analogy with (2),

$$A_{orb} = \cos \alpha_{orb} \cot \delta_{orb}, \qquad B_{orb} = \sin \alpha_{orb} \cot \delta_{orb}. \quad (6)$$

The coordinates of the two nodal points at which the orbit plane and the equatorial plane cross each other can be determined by equating (1) with (5). One set of these coordinates, α_{node}, δ_{node}, describes the unit vector Ω_{node} of the orbit plane's ascending node on the equatorial plane at the time of initial disruption which is calculated as a cross product

$$\Omega_{node} = \nu(\omega_{rot} \times \omega_{orb}), \quad (7)$$

where $\nu > 0$ is another normalization constant. The rotation parameters I and Φ are determined by the following dot-product expressions involving the four unit vectors:

$$\cos I = \omega_{rot} \cdot \omega_{orb}, \qquad \cos \Phi = \Omega_{node} \cdot \Omega_{jov}, \quad (8)$$

where the range of I is from 0° to 180°, the range of@ from 0° to 360° (Fig. 6). When $\omega_{rot} \cdot \Omega_{jov} > 0$, then $\Phi < 180°$ and vice *versa.*

Table 3. Solutions for the progenitor's rotation vector from information on secondary fragmentation events.

Fragments included	Northern pole of rotation		Note
	α_{rot}	δ_{rot}	
BCDFJMNP1P2Q2TUV	68?6 ±12?6	+77?8 ±3?4	
BFJMNP$_1$P$_2$Q$_2$TUV	68.9 ±14.0	+77.8 ±3.8	Case A
BCDFMNP2Q2UV	15.1 ±9.4	+76.8 ±1.8	
BFMNP$_2$Q$_2$UV	14.8 ±11.0	+76.8 *2.1	Case B
BFMNP$_2$UV	84.4 *14.3	+77.2 ±2.7	

6. Rotation vector and the effective diameter of the progenitor comet, and the quasi-continuous disintegration process

Various combinations of the 13 solutions selected for the fragments in Table 1 were used to determine the rotational parameters of the progenitor comet following the approach described in Sect. 5. The resulting coordinates of the northern rotation pole based on five sets of the fragments are listed in Table 3.

The first set comprises the preferred solutions for all 13 fragments included in Table 1. The second set excludes the two probable primary fragments, C and D. It is noted that their exclusion has practically no effect on the results. The third set keeps C and D in the sample, but excludes the tertiary fragments J, P_1, and T. Their removal can be justified by arguing that their parents, the secondary fragments N, P_2, and U, suffered more losses of the original angular momentum than the primary fragments, so" that these episodes in fact provide information that is somewhat inferior to that supplied by the events involving any of the primary fragments. We note that the elimination of J, P_1, and T from the set affects the rotation pole's right ascension.

Furthermore, one can argue that the primary fragments were gradually losing the "memory" of the initial angular momentum with every additional secondary-fragmentation event, in which case the episode that should provide the least reliable information is the last separation detected, that of Q_2 from Q_1. The fifth set, which amounts to the fourth set minus this event, yields (apparently by coincidence) results somewhat similar to those from the first and second sets. In summary, the pole coordinates cluster around two points, the right ascensions of which are, respectively, near 70–80° and 15°, while the declinations are always between +76° and +78°. No two solutions in Table 3 yield points that are farther apart from each other than 15°. In the following we derive our further

Table 4. Rotation parameters of the progenitor comet.

VECTOR ω_{orb}	VECTOR Ω_{jov}
α_{orb} = 181°.59	α_{jov} = 99°.85
δ_{orb} = +20°.26	δ_{jov} = −21°.27
VECTOR Ω_{node}	**PARAMETERS I, Φ**
Case A:	Case A:
α_{node} = 275°.7 ± 1°.5	I = 74°.8 ± 2°.7
δ_{node} = +10°.9 ± 3'.8	Φ = 191°.7 ± 3°.4
Case B:	Case B:
α_{node} = 272°.6 ± 0°.9	I = 82°.6 ± 1°.9
δ_{node} = +2°.8 ± 2°.4	Φ = 199°.7 ± 2'.3

results on two assumptions regarding the rotation vector: Case A, which is identical with the second set and is based on the 11 secondary and tertiary fragments and Case B, which is equal to the fourth set and is based on the eight secondary fragments. Comparing these results with the rotation vector for the nominal model of Shoemaker-Levy 9 that we formulated in Paper 1, we find that the difference (between the opposite poles) is 29° for Case A and merely 18° for Case B.

The rotation parameters I and Φ calculated for the two cases together with the directions of the relevant vectors (Sect. 5) are listed in Table 4. The derived obliquity indicates that the progenitor comet had its spin axis tilted some 7-15° to the jovicentric orbit plane near perijove, making an angle of ~70° to ~80° with the direction to Jupiter at perijove, as illustrated in Fig. 7.

Having established the initial spin-vector orientation, we next address the significance of the initial rates at which the fragment pairs are found to have separated (Table 1). Consider first an oversimplified model for a spherical nucleus of mass M, bulk density ρ, diameter D, and negligibly low tensile strength $\sigma_{tens} \to 0$. In order for a particle at the surface to escape, it need be given a critical velocity V_{crit} that is to satisfy a condition

$$\tfrac{1}{2}V_{crit}^2 = -U = \frac{2GM}{D} = \tfrac{1}{3}\pi G\rho D^2, \tag{9}$$

where U is the gravitational potential of the particle on the surface and G the universal constant of gravitation.

Next we relax the constraint of negligible strength and consider a *rotating* nucleus of the same density, diameter, and total mass, but of variable tensile strength. For a small piece of the nucleus to be at the point of breaking away due to rapid rotation, the tangential rotational velocity V_{tens} must satisfy a relation $\sigma_{tens} = \frac{1}{2}\rho V_{tens}^2$, where σ_{tens} is the local effective tensile strength. In order for the piece not only to break away but also to escape, the condition for the critical velocity depends on the fraction $\beta < 1$ of the energy that is lost due to friction, thermal effects, etc. during the breakup and on the relation between the gravitational and the cohesion terms. When $4GM/DV_{tens}^2 > 1-\beta$, the condition for the critical velocity becomes

$$\tfrac{1}{2}V_{crit}^2 = \frac{2GM}{D} + \tfrac{1}{2}\beta V_{tens}^2 = \tfrac{1}{3}\pi G\rho D^2 + \beta\frac{\sigma_{tens}}{\rho}. \tag{10}$$

When $4GM/DV_{tens}^2 \leq 1-\beta$, the condition is simply

$$V_{crit} = V_{tens}. \tag{11}$$

For a rotationally stable object the spin rate is below the critical limit and no piece can break away. When σ_{tens} is suddenly reduced, at least at some locations on the nucleus, due for example to the development of internal and superficial cracks caused by the jovian tides, the rotational tension may locally exceed the strength and a breakup becomes possible. The conclusion that Jupiter's tidal forces extensively cracked the nucleus of the progenitor but did not break it apart is used in Sect. 8 as a major argument in our formulation of a new model for comet Shoemaker–Levy 9. Hence, the relationship between the tidal and the rotational (and thermal) forces plays a major role in our considerations.

Next, we relax the unrealistic constraint of spherical shape for the nucleus fragments. It turns out that the gravitational potential at the surface of a body of any shape can be written in the form

$$-\frac{2GM}{D}\theta, \tag{12}$$

where D is now the object's characteristic dimension and θ is a dimensionless parameter that depends on the object's shape and the location of the potentially separating mass on the surface. Hence, with these minor modifications the conditions (10) and (11) are valid quite generally.

Because the progenitor comet's spin vector is found to have nearly coincided with the jovicentric orbital velocity vector at perijove, of particular interest are disk-shaped fragments rotating along an axis that is aligned approximately with the disk's effective diameter D (Fig. 7). Let the disk's average thickness be t and its characteristic thickness-to-diameter ratio $f = t/D$, which is typically much smaller than unity. In analogy to (10), one finds that when $\pi G\rho f D^2\theta/V_{tens}^2 > 1-\beta$, the condition for the critical velocity in the case of a disk-shaped nucleus is

$$\tfrac{1}{2}V_{crit}^2 = \tfrac{1}{2}\pi G\rho f D^2\theta + \tfrac{1}{2}\beta V_{tens}^2. \tag{13}$$

When $\pi G\rho f D^2\theta/V_{tens}^2 \leq 1-\beta$ the condition coincides with that of (11).

Let us consider two points on the disk's surface. One of them, point A in Fig. 7, is situated at a distance of $\frac{1}{2}t$ from the center along the line normal to the disk's base and passing through the center. The parameter θ for this point A is

$$\theta = \sqrt{1+4f^2} + 2f + \frac{1}{2f}\ln\left(2f + \sqrt{1+4f^2}\right). \tag{14}$$

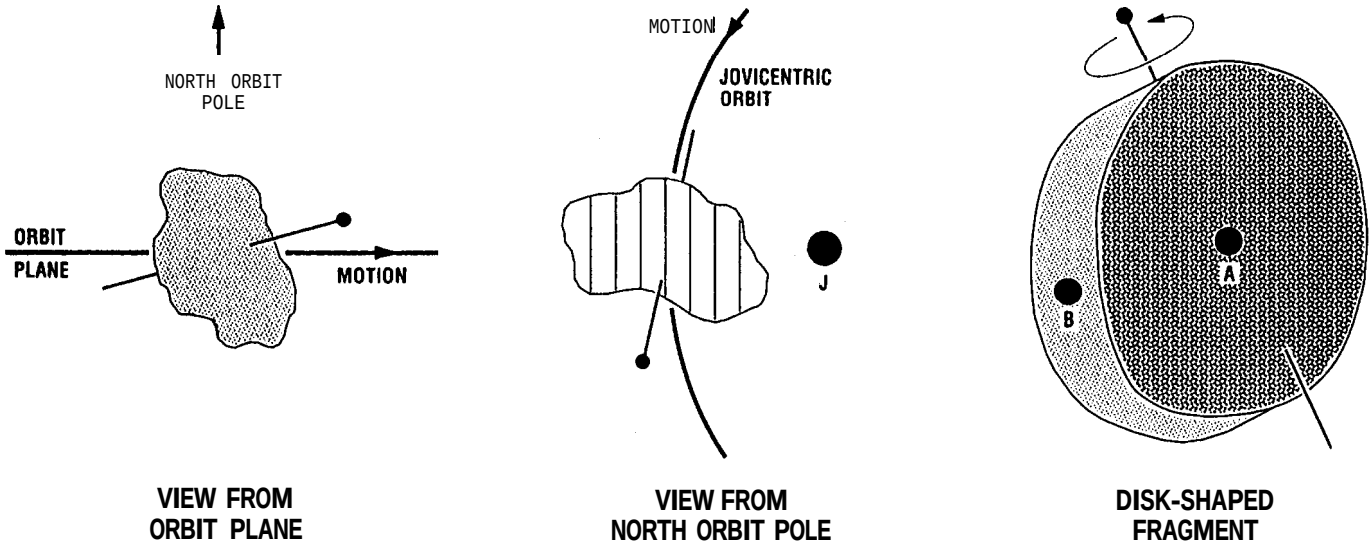

Fig. 7. The progenitor comet's rotation-vector orientation (Case A) at perijove (J = Jupiter): schematic views in the orbit plane in the direction of Jupiter (left) and normal to the orbit plane (middle). The dotted end of the spin axis refers to the northern pole. The fine crossbars across the comet's contour in the middle panel represent the planar sections along which a homogeneous nucleus would tend to crack due to the jovian tides that peak sharply at perijove. Rotational tension separates the cracked nucleus into several disk-shaped fragments along the cracks. One such spinning disk-like fragment is shown schematically on the right. At the points A and B the gravitational potentials are given by (12), with θ from, respectively, (14) and (15).

The second point, B in Fig. 7, is one of the points midway between the two planar surfaces of the disk. The distance of any such point from the disk's center is $\approx \frac{1}{2}D$ (the disk's planar surfaces are assumed to circular only in the first approximation) and the parameter θ is expressed by an integral

$$\theta = \frac{1}{\pi f}\int_0^1 \frac{dx}{x^2} \times \int_{-1}^{1} \arctan\left[\frac{2fx^2}{1-xy}\,\frac{\sqrt{1-y^2}}{\sqrt{1-2xy+x^2(1+f^2)}}\right] dy. \quad (15)$$

The derived separation velocities $V_{\rm sep}$ offer robust estimates for the critical velocities $V_{\rm crit}$ necessary for the secondary-fragmentation episodes to occur. Although one expects that $V_{\rm sep} > V_{\rm crit}$ for a successful separation, the calculated values of $V_{\rm sep}$ cannot be very different from $V_{\rm crit}$ for two reasons: one, the calculated separation velocity is that "at infinity" and therefore somewhat lower than the true separation velocity at the surface of the parent fragment; and, two, the fragmentation event would have occurred earlier, thus preventing $V_{\rm sep} >> V_{\rm crit}$ from ever materializing. This argument is based on our tacit premise that cracks were continuing to propagate throughout the nucleus during the post-encounter period, with the tensile strength of both the parent and the daughter fragments gradually decreasing with time. Compelling, straightforward evidence for this kind of progressive disintegration is provided by the disappearing condensations J, M, P_1, P_{2b}, or G_2. As secondary fragments are released one by one, the mass and the dimensions of the surviving parent fragments decrease with time. Hence, $V_{\rm crit}$ decreases with time, because $\sigma_{\rm tens}$, M, and D all decrease with time. Although some scatter resulting from the unevenness in the initial dimensions and irregular shape of the various fragments must be present, we would expect that *the separation velocity in secondary-fragmentation events should systematically decrease with time.* Agreement between this prediction and the data derived from the observations in Fig. 5 is striking,

The next and final task in this section is the examination of constraints on the effective dimensions of the progenitor comet's nucleus. Important information comes from considerations of the jovian tidal forces. Assuming a nucleus of 10 km in diameter and 0.2 g/cm^3 in bulk density, Sekanina (1996) calculated that the peak tidal stress at perijove amounted to 0.0038 bar, which, as we now argue, almost (but not quite) broke the nucleus apart. Thus, the comet's tensile strength must have been just slightly greater than this value. Since it varies as the product of the bulk density and the square of the diameter, the equivalent tidal stress exerted on the nucleus of 1.5 km in diameter and 0.6 g/cm^3 in density (Asphaug and Benz 1996) is merely 0.00026 bar. However, Greenberg *et al.* (1995) calculate that aggregate cometary material consisting of submicron-sized interstellar grains should have a tensile strength of $\sim$0.003 bar or greater. Consequently, the nucleus of the size advocated by Asphaug and Benz could not split tidally at all. The only recourse one has in the case of a diameter <<10 km is to postulate an unphysical, strengthless model.

Uncertainties in the tensile strength of the fragments are too high to allow us to derive a reliable effective nuclear diameter from these constraints in a general case. However, if one neglects energy losses ($\beta \rightarrow$ O) during a breakup at a plausible point, marked B in Fig. 7, the disk-shaped model for the primary fragments yields for the ratio of D/V_{crit} values of 14.1, 10.2, 8.6, and 7.6 km/m/s for an assumed thickness-to-diameter ratios f of 0.1, 0.2, 0.3, and 0.4, respectively. As long as $\beta V_{tens}^2 << V_{crit}^2$, *these* numbers offer relatively tight upper limits to the effective diameters of disk-shaped fragments. Note that only for the primary fragments near the middle of the train will the derived diameters be approximately equal to the (polar) diameter of the progenitor nucleus, while for the others, especially W, they will be smaller. With the separation velocities of 1.6–1.7 m/s for the two most relevant secondary-fragmentation events '(B from H and F from K), the derived upper bounds are well in excess of 10 km in the entire range of considered thickness-to-diameter ratios. That the actual diameter could not be *much* smaller than 10 km becomes obvious, when one calculates the corresponding rotation period. For an equatorial rotational velocity of 1.6 m/s, the spin period is found to be ~5.5 hours for D = 10 km, but a ridiculously small value of 49 minutes(!) for D = 1.5 km.

Our present results thus provide strong evidence that the progenitor nucleus of Shoemaker–Levy 9 had been a rapid rotator and that its rotation played major roles both in the object's initial disruption and in the subsequent sequence of secondary-fragmentation episodes. Unless the fragments were inexplicably spun up during the initial disruption, the comet must have been in the state of internal tensile stress before its encounter with Jupiter and it was only its tensile strength that prevented its earlier splitting. A significant loss of this resistance, due to the jovian tidal action in the immediate proximity of the 1992 peri-, jove, triggered the spectacular "chain" of episodes whose products were observed worldwide as constituent parts of what can, without exaggeration, be called the event of a millennium.

7. Orientation of the nuclear train and additional information on the primary fragments and the progenitor nucleus

In Paper 1, extensive experimentation with our ephemeris-determination software led us to a conclusion that the time of disruption of cornet Shoernaker-Levy 9 determined the temporal variations in the position angle of the nuclear train. This effect was found to be asymmetric in that the position angles (at any particular time) implied by a breakup at the same jovicentric distance before and after perijove do not match. Accordingly, the observed variations in the position angle of the on-train fragments could be exploited to derive an effective time of the initial disruption.

We also showed in Paper 1 that from the known time of initial disruption and angular length of the nuclear train at any later time one could determine the dependence between the size of the progenitor nucleus (along the radius vector from Jupiter) and the increment in the orbital velocity involved, Thus, the dimensions of the comet could *not* unequivocally be determined in this fashion without additional information.

The sample of position-angle observations in Paper 1 consisted of only 42 measures between discovery and mid-January 1994. This set was later extended to 144 data points covering the entire period of observation and the results of this unpublished work were reported only briefly (Sekanina 1996). As a result of this extension the initially derived breakup time of 2.2 hours after perijove was revised to 2.5 hours after perijove; the estimated uncertainty in both cases was ±0.5 hour.

We now introduce a few changes in the procedure of calculating the position angles of the train. First of all, we use the definitive orbital elements from Paper 2, which were not available for the earlier analyses. The train's position angle is now referred to fragment K, rather than Q, so as to reckon it from a point as close to the middle of the train as possible. The separation from K at the time of disruption, used in the position-angle determination, is calculated from each fragment's predicted impact time (which is constant) rather than from its observed offsets (which vary with time), Finally, we check the results based on the set of the eight "standard" fragments used before (E, G, H, K, L, Q, S, and W) by repeating the procedure with an eleven-fragment set (adding .4, C, and D to the standard set). Unfortunately, only 41 data points then qualify by offering sufficiently high positional accuracy.

Table 5 illustrates the superiority of the results based on the standard, eight-fragment set. The minimum on the curve of the sum of squares of the position-angle residuals is very well defined and the distribution of the residuals is symmetric, with the average residual attaining zero at about the same assumed time of disruption for which the sum of squares of the residuals reaches its minimum. With its formal error, the adopted time of initial disruption is 3.1 ± 0.2 hours after perijove. One notices that a breakup 12 hours after perijove provides a better fit than one at perijove and that a breakup 24 hours after perijove offers a better fit than a breakup 1 hour before perijove.

Even though the solution based on the set of eleven fragments is distinctly inferior, it is encouraging that it yields a time of disruption of 2.3 ± 0.7 hours after perijove, which overlaps the above result. *The comet's initial disruption did not occur at perijove but some 3 hours or so later.*

As a byproduct of the nuclear-train analysis we obtained extensive tabulations of the offsets of the individual fragments from the mean position of the train. The average offsets (positive to the north of the train, negative to the south) are listed in Table 6 separately for

Table 5. Sum of squares of the residuals from the nuclear train's position angles as a function of the assumed effective time of initial disruption, based on the sets of 8 fragments E-W (144 observations) and 11 fragments A-W (41 observations).

Set of on-t rain fragments employed	Assumed time of disruption (hr)[a]	Sum of squares of residuals in position angle (deg^2)	Calculated average residual in position angle (deg)
E-W	-1	37.8373	-0.33
	0	18.3192	–0.22
	+1	7.0933	–0.11
	+2	3.9837	-0.05
	+3	3.3026	0.00
	⟹ +3.1	3.2976	0.00
	+3.2	3.3011	+0.01
	+4	3.5587	+0.03
	+5	4.2682	+0.06
	+7	6.3588	+0.10
	+12	12.9086	+0.18
	+24	29.3044	+0.30
	+48	58.6515	+0.44
A-W	+1	0.9078	–0.09
	+2	0.7657	-0.07
	+2.2	0.7602	–0.06
	+2.3	0.7606	-0.06
	+2.4	0.7599	–0.06
	+2.5	0.7622	–0.06
	+3	0.7804	–0.05
	+4	0.8541	–0.03
	+5	0.9530	–0.02

[a] Reckoned from perijove: negative is a preperijove time, positive are post-perijove times.

the pre-conjunction (until the end of July 1993) and post-conjunction (from December 1993 onward) periods. On the left-hand side of the table we show the 12 on-line fragments while on the right-hand side, the 12 off-line fragments (not listed is P_{2b}). The rows "8" and "11" list the offsets from the train that is defined by, respectively, the eight fragments E-W and the eleven fragments A–W. The distribution of the pre-conjunction offsets confirms — with a few unimportant exceptions —- the conclusion from Paper 1 that the offsets of the on-line fragments are within their errors while the offsets of the off-line fragments exceed their errors by a factor of up to several.

The post-conjunction results also confirm that the secondary and tertiary fragments deviated significantly toward the north of the nucleartrain, but this time there are no exceptions. Because all these fragments originated in the events of secondary fragmentation, one can argue that, as a rule of thumb, *later separations from the parent object statistically correlate with more prominent northerly offsets* in the post-conjunction period. In fact, five of the nine off-train fragments for which this exercise could be carried out — F, N, PI, P_2, and T — have a post-conjunction average-offset rate between +0.03 1 and +0.042 arcsec per day of separation time reckoned from the 1992 perijove (fragments J, M, and G_2 have insufficient data), The mean offset rate for the nine off-train fragments is +0,028+ 0.016 arcsec per day of separation time.

Turning now to the on-train fragments in the post-conjunction period we find that their offsets from the train based on the eight-fragment set range from –0.25 to +0.46 arcsec, equivalent, using the above derived rates, to a period of ~20 days during which the breakup events that gave birth to the 12 primary fragments should have occurred. Although this is almost certainly a crude overestimate, an indication that the average offsets of these fragments may not overlap each other provides evidence that the initial disruption could have been a sequence of breakups rather than a single event. Support for this conclusion is offered by the identity of the on-train fragments of extreme southerly and northerly offsets, as discussed in the next paragraph. Another argument is based on the evidence already presented in Sects. 4.1, 4,3, and 4.4 and further discussed below, The crude estimate of 20 days is the basis for our claim in Sect. 4.17 that all the on-train fragments existed as independent fragments by the end of July 1992. A more conservative estimate for the duration of the presumed initial sequence of breakups probably is just a few days at the most.

Returning to column 4 of Table 6, we would like to call attention to a pair of the on-train fragments G and K. They have the largest *southerly* offsets from the train, comparable with their 1σ in the "8" sample and with their 2σ in the "11" sample. According to our rule of thumb, these two fragments, which were among the three most massive ones upon impact, were probably involved in the earliest event of the presumed sequence of breakups. Another group of noteworthy objects includes D, C, and A, which among the on-train fragments have the largest *northerly* offsets in the "8" sample, comparable with or exceeding their 1σ. Their offsets in the "11" sample, though somewhat smaller (for obvious reasons), also indicate a systematic trend. According to our rule of thumb, these objects should have been among the last on-train fragments to separate from the remnants of the progenitor's comet, This conclusion is consistent with our findings in Sects. 4.1, 4.3, and 4.4.

A fair description of the purpose for determining the average offsets of individual fragments from the mean train is to say that they offer a crude indication of which fragments separated earlier and which later. However, the offsets do not provide any useful information on the actual separation times of individual fragments and, consequently, they cannot be used to establish a breakup sequence.

Clearly, the discrimination of the fragments into their on-train and off-train categories is independent of whether or not A, C, and D are added to the eight standard frag-

Table 6. Offsets from nuclear train defined by 8 fragments E-W and by 11 fragments A-W.

On-train fragment		Pre-conjunction period: Offset from train (arcsec)	Pre-conjunction period: Number of data	Post-conjunction period: Offset from train (arcsec)	Post-conjunction period: Number of data
A	"8"	+0.03 ± 0.06	4	+0.29 ± 0.32	40
	"11"	0.00 ± 0.03	4	+0.08 ± 0.25	37
C	"8"	+0.06 ± 0.07	5	+0.44 * 0.35	53
	"11"	+0.06 ± 0.05	4	+0.16 ± 0.24	37
D	"8"	+0.02 ± 0.07	4	+0.46 ± 0.40	47
	"11"	−0.01 ± 0.05	4	+0.23 ± 0.29	37
E	"8"	-0.02 ± 0.16	52	+0.28 ± 0.38	92
	"11"	–0.01 ± 0.05	4	–0.01 ± 0.18	37
G	"8"	−0.02 ± 0.15	52	−0.22 ± 0.25	92
	"11"	-0.01 ± 0.02	4	−0.36 ± 0.19	37
H	"8"	+0.11 ± 0.17	52	0.00 ± 0.29	92
	"11"	0.00 ± 0.02	4	-0.08*0.16	37
K	"8"	+0.07 * 0.20	52	−0.25 ± 0.21	92
	"11"	0.00 ± 0.06	4	−0.27 ± 0.13	37
L	"8"	−0.21 ± 0.19	52	−0.04 ± 0.38	92
	"11"	−0.12 ± 0.03	4	−0.13 ± 0.16	37
Q[a]	"8"	+0.04 ± 0.16	52	+0.16 ± 0.28	92
	"11"	+0.06 ± 0.04	4	+0.25 ± 0.22	37
R	"8"	+0.15 ± 0.21	23	−0.08 ± 0.38	84
	"11"	+0.02 ± 0.06	4	−0.07 ± 0.21	37
S	"8"	−0.01 ± 0.18	52	+0.10 ± 0.27	92
	"11"	+0.02 ± 0.07	4	+0.20 * 0.13	37
W	"8"	+0.03 ± 0.14	52	–0.06 ± 0.34	92
	"11"	0.00 ± 0.05	4	–0.07 * 0.19	37

Off-train fragment		Pre-conjunction period: Offset from train (arcsec)	Pre-conjunction period: Number of data	Post-conjunction period: Offset from train (arcsec)	Post-conjunction period: Number of data
B	"8"	+0.47 ± 0.04	4	+1.46 ± 0.43	60
	"11"	+0.45 ± 0.04	4	+1.27 ± 0.31	37
F	"8"	+0.08 ± 0.14	8	+1.67 ± 0.57	71
	"11"	+0.15 ± 0.04	4	+1.56 ± 0.43	36
G_2	"8"		0	+2.26 ± 0.58	4
	"11"		0	+2.30 ± 0.54	3
J	"8"	+0.28 ± 0.06	4	–	0
	"11"	+0.27 ± 0.07	4		0
M	"8"	+0.34 ± 0.15	4		0
	"11"	+0.34 ± 0.14	4		0
N	"8"	+0.11 * 0.09	6	+1.39 ± 0.57	47
	"11"	+0.11 ± 0.11	4	+1.68 ± 0.64	29
P_1	"8"	(+0.05)	1	+4.24 ± 0.99	26
	"11"		0	+4.17 ± 1.14	17
P_2	"8"	+0.29 ± 0.14	11	+3.86 ± 0.87	61
	"11"	+0.27 ± 0.05	4	+3.58 ± 0.81	35
Q_2	"8"	(+0.18)	1	+0.88 ± 0.22	6
	"11"		0	+0.83 ± 0.23	4
T	"8"	+0.36 ± 0.10	3	+3.67 ± 0.74	35
	"11"	+0.37 * 0.10	3	+3.78 ± 0.80	25
U	"8"	+0.11 ± 0.11	7	+1.47 ± 0.42	17
	"11"	+0.12 ± 0.13	4	+1.54 ± 0.45	14
V	"8"	+0.09 ± 0.16	4	+1.35 ± 0.47	48
	"11"	+0.10 ± 0.17	4	+1.47 ± 0.41	34

[a] Or Q_1, when Q is resolved into two components.

ments to define the train's orientation. However, since A, C, and D are offset somewhat to the north of the train, their incorporation among the fragments determining the train's orientation leads to position angles that, on the average, are systematically smaller by 0°.05 or so. It is interesting that this effect did not show up at all in the effective time of disruption; if it did, the A–W set should have yielded a later time of disruption than did the E-W set in Table 5. The reason for this is that the solution was dictated primarily by the choice and temporal distribution of the 41 data that made up the sample based on the A-W set (relative to the sample of 144 data based on the E-W set), an effect that overshadowed that of the slight difference in the train's slope.

Having determined the effective time of initial disruption and the spin-axis orientation at that time, and having set fairly tight limits on the rotational velocity of the progenitor comet, we are now in a position to constrain the comet's original nuclear dimensions more tightly than we were able to do before. This is accomplished entirely on the basis of the model worked out in Paper 1. With the known spin vector, the problem is reduced to finding (i) the increment in the orbital velocity contributed by rotation at the time of disruption and (ii) the nuclear diameter, defined as the separation between the subjovian and antijovian points on the nuclear surface, such that its effect combined with that in the orbital velocity satisfies the known dynamical parameters of the nuclear train. Even though the velocity increment involved is along the orbital velocity vector, the solution can actually be carried out in the RTN coordinate system.

In the RTN system referred to the center oft he comet's nucleus and oriented with respect to Jupiter, the unit vector of the subjovian point on the surface of the nucleus has the components {–1, O, O}, the unit vector of the antijovian point, {+1, O, O}. Approximating the disruption as a single event that occurred at a jovicentric true anomaly u_0, we have for the cometocentric latitute of the subjovian point

$$\phi_{\rm sub} = \arcsin\left[\sin I \sin(\Phi + u_0)\right] , \qquad (16)$$

where I and Φ are the rotation parameters introduced in Sect. 5. The cometocentric latitute of the antijovian point is $-\phi_{\rm sub}$. The radial components of the rotational velocity at the subjovian and antijovian points are zero. The normal component of the velocity has no effect on the solution (as we showed in Paper 1) and the only velocity contribu-

tion comes from the transverse component. The expression for this component at the subsolar point is (Appendix B of Paper 1)

$$(V_{sub})_{transv} = \frac{2\pi}{P_{rot}} \Re_{sub} \cos I, \quad (17)$$

where $\Re_{sub}$ is the distance of the subsolar point from the rotation axis at the time of disruption. This velocity component at the antijovian point has the opposite sign. With a quasi-spherical approximation the equivalent equatorial radius is $R = \Re_{sub} / \cos \phi_{sub}$. If we approximate the (equatorial) rotation velocity by a separation velocity V_{sep} derived from the secondary-fragmentation events, we can write Eq. (17) in the form

$$(V_{sub})_{transv} = -V_{sep} \cos \phi_{sub} \cos I. \quad (18)$$

This technique was employed on the assumption that all the on-train fragments separated at 3.1 hours after perijove, at which time the comet's jovicentric true anomaly was $u_0 = +116°.6$, The calculations were carried out for three values of the equatorial rotational velocity — 1.0, 1,3, and 1.6 m/s (the limits approximately coinciding with the derived mean and peak separation velocities V_{sep} derived in Sect. 4.17) — and for Cases A and B (Table 3) of the spin-axis orientation. The two scenarios yield for the subjovian point's latitude, respectively, $\phi_{sub} = -490.2$ and -43°.2. Consistent with the practice employed in determining the nuclear-train orientation, each solution was required to satisfy the times of impact for fragment A (which was used to approximate the subjovian point at the time of disruption) and fragment W (which was taken to approximate the antijovian point), based on their orbital elements in Paper 2. From our previous findings in this section, the separations of fragments A and W from K were taken to be, respectively, 0.9455 and 1.0545 mean radii,

Our computations show' that acceptable solutions result only with the rotation sense requiring that the separation points be located on the antisolar side of the parent objects (Sect. 5). The opposite rotation sense yields unacceptably large dimensions for the progenitor nucleus, on the order of several tens of kilometers, The effective diameter and the corresponding rotation period in the accepted scenario for the six combinations of the spin-axis orientation and rotational velocity are listed in Table 7. Evidently, Case A yields a faster rotator of slightly smaller dimensions. Even though still involving approximations (e.g., neglecting the possibility of the disruption consisting of a series of separate events), the table nonetheless covers a wide range of plausible solutions, The preferable solutions are those calculated for the higher velocities. These results fully confirm our earlier findings based on independent evidence (Paper 1 and Sect, 6 of this study) that the nucleus of the progenitor comet was a fast rotator approximately 10 km in diameter.

Table 7. Effective diameter and rotation period for the nucleus of the progenitor comet.

Rotation velocity approximate ion, V_{sep} (m/s)	Diameter (km)		Period (hr)	
	Case A	Case B	Case A	Case B
1.6	9.3	12.6	5.1	6.9
1.3	10.7	13.3	7.2	8.9
1.0	12.0	14.1	10.5	12.3

8. Critique of existing hypotheses and a new model for the comet's fragmentation. Summary and conclusions

The prime objectives of this paper are to appraise the existing hypotheses for the splitting of Shoemaker–Levy 9 and to formulate a new model that is fully consistent with the results of analysis of the observed phenomena. First we list our findings: (i) the orientation of the nuclear train implies that the 12 primary fragments were released not in a single event but, more probably, in a sequence of discrete episodes effectively centered on a time some 3.1 hours after perijove; (ii) the effect in the nuclear-train orientation is exceedingly nonlinear in that the first episode could not have taken place much sooner than perhaps a fraction of one hour before this effective time, while the last episode could possibly occur as late as a few days afterwards; (iii) discrete episodes of secondary fragmentation, giving birth to the off-train fragments, took place, at a gradually decreasing rate, over a period of many months following the progenitor comet's initial disruption; (iv) the separation-velocity vectors of the secondary (and tertiary) fragments are distributed along a great circle in projection onto the plane of the sky, pointing to the approximate conservation of the progenitor comet's angular momentum; (v) the derived orientation of the spin axis shows that it was located almost in the jovicentric orbit plane and approximately aligned with the orbital velocity vector at perijove; (vi) the rotation sense indicates that the off-train fragments separated from areas of their parents that were at the critical times located on the antisolar side; and (vii) the separation velocities of the secondary and tertiary fragments are found to have decreased systematically with time, dropping from the peak values near 1.6–1.7 m/s for events that occurred within 1–2 months of perijove to ~0.4 m/s some three-quarters of a year later.

The rapid rotation with a strongly tilted axis rules out the strengthless aggregate models developed for the nucleus of comet Shoemaker-Levy 9 by Solem (1995) and by Asphaug and Benz (1996). The authors of these nearly identical paradigms were aware of their concept's sensitivity to nucleus rotation and discussed the effects. Asphaug and Benz, who examined scenarios for an assumed rotation period of 9 hours, stated explicitly that in none of their solutions "did a comet with significant rotation out

of the plane of the orbit result in uniform clumps comparable to SL9." Solem modelled configurations with the spin axis in the orbit plane only for a slowly rotating comet, with a spin rate assumed to amount to one third the critical rate for centrifugal breakup or less. The general conclusion is that (fast) rotation out of the plane of the orbit hinders clumping subsequent to breakup and the result is essentially a single, massive central condensation, in sharp contradiction to the appearance of Shoemaker–Levy 9.

In Paper 1 we proposed that the observed orientation of the nuclear train defined the point of dynamical separation of the primary fragments. In the light of evidence from our comprehensive analysis of the secondary-fragmentation events, which were positively nontidal in nature, it is now necessary to revise the model for the comet's disruption. The major questions concern the interaction between rotational and thermal stresses and the jovian tidal forces as well as their separate roles in the progenitor comet's disintegration.

The fundamental feature of our new model is a deemphasized role for the jovian tidal forces. We submit that *due to the jovian tides the nucleus of the progenitor comet suffered extensive cracks throughout much of its interior but was not in the process of physical disruption until after perijove.* We argue that *the comet then began to split along the planes of severe tidally-triggered cracks due to its rapid rotation.* This interpretation not only replaces the relatively ambiguous concept of dynamical separation with a much more straightforward concept of physical splitting but is also supported by relatively high separation velocities involved. In addition, it shows that the events of secondary fragmentation can be understood as stochastic manifestations of the continuing process of disintegration that began with the sequence of early breakups and then gradually tapered off.

The fact that separations of the secondary and tertiary fragments are found to have taken place from the antisolar side of the parent fragments must be explained by any plausible model. Otherwise it would have to be postulated that the comet's continuing disintegration was spontaneous and the observed strong systematic trend for the daughter fragments to detach from their parents in north-easterly directions would remain unexplained.

The evidence from fragment P_1 is inconclusive. Nominally, the preferred solution (Table 1), which is based on the three available HST data, predicts that at the time of separation of P_1 from P the Sun was 12° *above* the local horizon. However, the other tabulated solution that is also based on three HST data (but assumes Q to be the parent) predicts a separation time at which the Sun was *37° below* the horizon. Thus, the exception offered by fragment P_1 is apparently not significant because all solutions for this condensation involve large uncertainties.

At first glance, separations of the secondary and tertiary fragments from the antisolar side of the parent objects are counterintuitive. It is fair to say that this evidence suggests that there is no direct role for solar radiation in the mechanism. However, there may be an indirect effect and we submit that in detaching a fragment the stresses due to rapid rotation could be assisted by thermal stresses near the surface, The presumed high porosity implies a low thermal inertia, which allows temperature gradients to develop in the surface layer of the parent fragment in locations that rotate into and out of sunlight (e.g., Kührt 1984). Strong temperature gradients are believed to develop only in a very thin layer (e.g., Brin and Mendis 1979, Fanale and Salvail 1984, Rickman and Fernández 1986), because their buildup is impeded by vapor diffusion of sublimating volatile materials from below the inert mantle. However, this impediment would disappear in the absence of activity. Although the role of thermal stresses in a highly porous medium has never been investigated and their contribution to the process of secondary fragmentation in comet Shoemaker–Levy 9 remains speculative, we remark that with the values for Young's modulus, Poisson's ratio, and the coefficient of linear expansion that McCrosky and Ceplecha (1970) recommended for meteors, the dominant component of thermal stresses amounts to $\sim$3 bars per degree of a temperature difference.

Closer scrutiny suggests that separations of small masses from the antisolar side of a cometary nucleus are not entirely unexpected. From temperature profiles in a consolidated dust mantle on the surface of a nucleus modelled by Fanale and Salvail (1984), Sekanina and Larson (1986) calculated thermal stresses at several points during the diurnal cycle, establishing both their nature (tension vs. compression, radial vs. tangential) and magnitude. It was found that tangential stresses, while strongly depth dependent, exceeded radial stresses by orders of magnitude. For our present considerations the most interesting finding is the difference between the sunlit and dark sides. On the sunlit side the prevalent thermal stresses were always compressive, working against rotational tension. By contrast, the tangential stresses on the antisolar side, although smaller in magnitude, were predominantly tensile, enhancing the effect from fast rotation. One would therefore be mistaken to assume that thermal stresses disappear when an area rotates out of sunlight.

Taking this information into account, it is plausible to argue that even a slight temperature gradient at the nuclear surface could generate thermal stresses that assist rotational forces in triggering, from time to time, the separation of a relatively small piece from the parent.

In July 1994 the individual fragments arrived at Jupiter in very different conditions. For days before impact the dust coma of each condensation became subjected to jovian-gravity driven progressive stretching, confirming that it consisted of a loose cloud of particulate. However, no stretching can be detected in the innermost, brightest part of the published images of several condensations, which retained the appearance of an unresolved dot (cf. the last HST frame of Q_1 and Q_2 in Fig. 2 of Weaver *et*

al. 1995, taken less than 11 hours before the crash of Q_2). Even though the digital charts of these images have never been properly analyzed, there is little doubt that large central objects still existed in both Q_1 and Q_2 at those late times. From unobstructed observations of the bolides and their explosions with the Galileo instruments (Chapman *et al.* 1995) and from detections of the expanding plumes of debris by the HST camera (Hammel *et al.* 1995), one can conclude that at least nine of the 12 on-train condensations contained massive central fragments upon impact. For the remaining three condensations, C, D, and S, there at least is information on their second precursors and impact sites (Paper 2 and Nicholson 1996).

Significantly, very little is known in comparison about the off-train condensations. Among the secondary fragments, the best data are for N from the Galileo imaging (Chapman *et al.* 1995) and from the impact site (Hammel *et al.* 1995), and for V from apparent observations of the first precursor (Nicholson 1996). In addition, a precursor was detected for Q_2 (Herbst *et* al. 1995), while impact sites and main events were reported for B and Q_2, a possible main event also for M. No information whatsoever is available on the tertiary fragments.

It seems that condensations N, Q_2, and V "landed" fairly large, probably subkilometer-sized fragments deep in the jovian atmosphere, while the central objects in the remaining condensations must have broken up tidally and/or due to atmospheric drag into still smaller pieces that completely burnt up high in the atmosphere with no detectable plumes. The comment by Beebe (1996) that the site of B was apparently located higher in the atmosphere than the other dark features is consistent with this scenario, In any case, the jovian tides, which began to affect the fragments *before* their atmospheric entry, must have played an important (and usually ignored) role in the final moments of the disintegration process.

It is not necessarily true that the entire mass of any off-train fragment ends up in small particulate. There may have survived perhaps as large as 10-meter-sized objects near the cores of condensations B, F, P_2, T, and others until their impacts. Yet, the motions of the *centroids* of condensations F, P_1, and P_2 must have been determined by the spatial distribution of centimeter-sized debris, therefore showing effects of solar radiation pressure. Although no such effects were detected in the motions of J, M, T, and U, this very well may be due to a small number of accurate measurements and the resulting inferior solutions that are available for these fragments.

Finally, a few comments on the nuclear fragmentation of Shoemaker-Levy 9 in the context of the problem of split comets in general and the so-called dissipating comets (Sekanina 1984), which also are fragments of comets that split long ago. The differences between the dynamical behavior of nontidally split comets and comets whose splitting involves tidal forces were recently addressed in some detail by Sekanina (1997). A new issue now raised by Shoemaker-Levy 9 is the nature of the deceleration in the equations of motion, For nontidally split comets, the deceleration of the secondary nuclei was interpreted as a differential nongravitational effect from directed outgassing. In this paper we show that the relative motions of the majority of fragments of Shoemaker-Levy 9 are affected by no detectable deceleration and that in the three exceptions the effect is apparently due to solar radiation pressure, so that no outgassing is required to explain this evidence. The question to address is whether the nongravitational effects detected in the relative motions of fragments of nontidally split comets could likewise represent signatures of solar radiation pressure rather than effects of outgassing. The answer to this question must be negative, because unlike in the three cases of fragments of Shoemaker-Levy 9, secondary nuclei of nontidally split comets are observed to depart from the main mass essentially along the projected antisolar direction. This represents a fundamental difference between the two types of split comets, even though the events of secondary fragmentation in Shoemaker–Levy 9 were also nontidal in nature. On the other hand, the basic *physical attributes* of fragments in their advanced phase of disintegration are always essentially the same for either kind of split comets as well as for the dissipating comets. Their demise is described by the loss of a central condensation, by an apparent expansion and elongation, and eventually by precipitous fading.

Acknowledgements. We thank Imke de Pater for communicating information on the impact of fragment B, as observed by her and her team with the W. M. Keck telescope, and for helpful discussions on the subject. This research was carried out at the Jet Propulsion Laboratory, California Institute of Technology, under contract with the National Aeronautics and Space Administration.

References

Asphaug, E., and Benz, W., Size, density, and structure of comet Shoemaker-Levy 9 inferred from the physics of tidal breakup. *Icarus* 121, 225-248, 1996.

Beebe, R. F., Growth and dispersion of the Shoemaker-Levy 9 impact features from HST images. In: *The Collision of Comet Shoemaker–Levy 9 and Jupiter,* K. S. Nell, H. A. Weaver, and P. D. Feldman, eds., pp. 307-328. Cambridge University, Cambridge, U. K., 1996.

Brin, G. D., and Mendis, D. A., Dust release and mantle development in comets. *Astrophys. J.*. 229, 402-408, 1979.

Chapman, C. R., Merline, W. J., Klaasen, K., Johnson, T. V., Heffernan, C., Belton, M. J. S., Ingersoll, A. P., and the Galileo Imaging Team, Preliminary results of Galileo direct imaging of S–L 9 impacts. *Geophys. Res. Lett.* 22, 1561-1564, 1995.

Chodas, P. W., and Yeomans, D. K., The orbital motion and impact circumstances of Comet Shoemaker–Levy 9. In: *The* Collision *of Comet Shoemaker-Levy 9 and Jupiter,* K. S. Nell, H. A. Weaver, and P. D. Feldman, eds., pp. 1-30. Cambridge University, Cambridge, U. K., 1996. (Paper 2)

de Pater, I., personal communication, 1997.

de Pater, I., Graham, J., and **Jernigan,** G., Periodic comet Shoemaker-Levy 9 (1993e). *IA U Circ. No. .6024, 1994.*

Fanale, F.P., and Salvail, J. R., An idealized short-period comet model: Surface insolation, H_20 flux, dust flux, and mantle evolution. *Icarus* 60, 476–51 1, 1984,

Graham, **J. R., de Pater, I., Jernigan, J. G., Liu, M. C., and Brown, M. E., The fragment** R collision: W. M. Keck telescope observations of SL9. Science 267, 1320-1323, 1995.

Greenberg, **J. M., Mizutani,** H., and **Yamamoto, T.,** A new derivation of the tensile strength of cometary nuclei: application to comet Shoemaker–Levy 9. *Astron. Astrophys.* 295, L35-L38, 1995.

Hammel, H. B., Beebe, R. F., Ingersoll, A. P., Orton, G. S., Mills, J. R., Simon, A. A., Chodas, P., Clarke, J. T., De Jong, E., Dowling, T, E., Barrington, J., Huber, L. F., Karkoschka, E., Santori, C. M., Toigo, A., Yeomans, D., and West, R. A., HST imaging of at mospheric phenomena created by the impact of comet Shoemaker-Levy 9. Science 267, 1288-1296, 1995.

Herbst, T. M., Hamilton, **D.** P., **Böhnhardt,** H., and Ortiz-Moreno, J. **L.,** Near infrared imaging and spectroscopy of the SL-9 impacts from Calar Alto. *Geophys. Res. Lett. 22, 2413-2416, 1995.*

Jewitt, D., Luu, J., and Chen, J., Physical properties of split comet Shoemaker–Levy 9. Bull. *Am. Astron.* Sot. 25, 1042, 1993.

Jewitt, D., and Trentham, N., Periodic comet Shoemaker-Levy 9 (1993e). *IA U Circ.* **No.** 5999, 1994.

Kührt, E., Temperature profiles and thermal stresses in cometary nuclei. *Icarus* 60, 512–521, 1984.

Lindal, G. F., Wood, G. E., Levy, G. S., Anderson, J. D., Sweetnam, D. N., Hotz, H. B., Buckles, B. J., Holmes, D. P., Doms, P. E., Eshleman, V. R., Tyler, G. L., and Croft, T. A., The atmosphere of Jupiter: An analysis of the Voyager radio science occultation measurements. *J. Geophys. Res.* 86, 8721-8727, 1981.

McCrosky, R. E., and Ceplecha, Z., Fireballs and physical theory of meteors. *Bull. Astron. Inst. Czech. 21, 271-296, 1970.*

Nicholson, P. D., Earth-based observations of impact phenomena, In: *The* Collision of *Comet Shoemaker–Levy 9 and Jupiter,* K.S. Nell, H. A. Weaver, and P. D. Feldman, eds., pp. 81-109. Cambridge University, Cambridge, U. K., 1996.

Nell, **K. S., and Smith, T. E.,** Periodic comet Shoemaker–Levy 9 (1993e). *IA U Circ.* No. 6010, 1994.

Rickman, **H., and Fernández, J. A.,** Formation and blowoff of a cometary dust mantle. in *The* Comet Nucleus *Sample Return* Mission, ESA SP-249, O. Melita, cd., pp. 185-194. ESTEC, Noordwijk, The Netherlands, 1986.

Scotti, J. V., personal communication, 1993.

Sekanina, **Z.,** The problem of split comets in review. In: *Comets,* L. L. Wilkening, eel., pp. 251-287. University of Arizona, Tucson, 1982.

Sekanina, **Z.,** Disappearance and disintegration of comets. Icarus 58, 81-100, 1984.

Sekanina, **Z.,** Effects of discrete-source outgassing on motions of periodic comets and discontinuous orbital anomalies. *Astron. J.* **105, 702-735, 1993.**

Sekanina, Z., Evidence on sizes and fragmentation of the nuclei of Comet Shoemaker-Levy 9 from Hubble Space Telescope images. *Astron. Astrophys.* **304**, 296–316, 1995.

Sekanina, **Z.,** Tidal breakup of the nucleus of Comet Shoemaker-Levy 9. In: *The* Collision *of Comet Shoemaker–Levy* 9 *and Jupiter,* K. S. Nell, H. A. Weaver, and P. D. Feldman, eds., pp. 55-80. Cambridge University, Cambridge, U. K., 1996.

Sekanina, **Z.,** The problem of split comets revisited. *Astron. Astrophys. 318, L5-L8, 1997.*

Sekanina, Z., Chodas, P. W., and Yeomans, D. K., Tidal disruption and the appearance of periodic comet Shoemaker-Levy 9. *Astron. Astrophys.* 289,607-636, 1994. (Paper 1)

Sekanina, **Z., Chodas, P. W., and Yeomans, D. K., Secondary fragmentation events of** comet **Shoemaker–Levy 9. In:** *Conference International sur la* Collision *SL9–Jupiter,* C. de Bergh and Th. Encrenaz, eds., p. IV-6 (abstract). Observatoire de Paris, Meudon, France, 1996.

Sekanina, **Z., and Larson, S. M., Coma morphology and dust-emission pattern of periodic comet Halley. IV. Spin vector refinement and map of discrete dust sources for 1910.** *Astron. J.* 92, 462-482, 1986.

Solem, J. C., Cometary breakup calculations based on a gravitationally-bound agglomeration model: the density and size of Shoemaker-Levy 9. *A stron. Astrophys. 302, 596-608, 1995.*

Takeuchi, S., Hasegawa, H., Watanabe, J.-i., Yamashita, T., Abe, M., Hirota, Y., Nishihara, E., Okumura, S.-i., and Mori, A., Near-IR imaging observations of the cometary impact into Jupiter. *Geophys. Res. Lett. 22,* 1581-1584, 1995.

Tholen, D. J., personal communication, 1994.

Weaver, H. A., A'Hearn, M. F., Arpigny, C., Boice, D. C., Feldman, P. D., Larson, S. M., Lamy, P., Levy, D. H., Marsden, B. G., Meech, K. J., Nell, K. S., Scotti, J. V., Sekanina, Z., Shoemaker, C. S., Shoemaker, E. M., Smith, T. E., Stern, S. A., Storrs, A. D., Trauger, J. T., Yeomans, D. K., and Zellner, B., The Hubble Space Telescope (HST) observing campaign on comet Shoemaker–Levy 9. *Science* 267, 1282-1288, 1995.

This article was processed by the author using Springer-Verlag LaTeX A&A style file *L-AA* version **3.**